PREDICTING TRIBOLOGICAL PERFORMANCE OF LIQUID LUBRICANTS AND COATED-SURFACES BY MACHINE LEARNING APPROACHES

BY

MUHAMMAD HAZMAN BIN SHARUDDIN

A dissertation submitted in fulfillment of the requirement for the degree of Master of Science in Engineering

Kulliyyah of Engineering
International Islamic University Malaysia

FEBRUARY 2025

ABSTRACT

Minimizing friction and wear between contacting surfaces is a central focus in tribology, especially in improving lubricants' performance for engine durability and reliability. Low-viscosity lubricants, while beneficial for fuel efficiency, present challenges in reducing friction and wear. The shift to low-viscosity lubricants, such as SAE 5W30 and SAE 0W20, raises concerns about increased surface contact and potential durability challenges, highlighting the need for advanced additives like graphene and fullerene, as well as coatings, to mitigate these issues, while leveraging machine learning to predict tribological performance and reduce resource-intensive experimental trials. Graphene and fullerene have gained attention as potential additives to enhance the tribological properties of lubricants This study investigates the effects of 0.005 wt.% graphene and fullerene in SAE 0W20 lubricant, along with six different coatings (TiN, AlTiN, CrN, TiAlSN, TiCN, and DLC-AlTiN) on steel block. The primary aim is to develop a dataset that explores the relationships between these additives and coatings with critical tribological parameters—coefficient of friction, wear area, and temperature. Using a rod and ring tribometer, this study measures the tribological performance, with SEM and EDX analyses for surface characterization. The findings indicate that graphene and fullerene additives significantly reduce friction and wear, with graphene showing better heat dissipation. The coatings, particularly CrN, reduce wear and friction, although CrN showed higher wear compared to others. Machine learning models, including Support Vector Regression (SVR), Random Forest (RF), and Decision Tree (DT), were used to predict the tribological parameters. RF outperforms SVR and DT in predicting both friction and wear area, while DT excels in predicting temperature. This research contributes to improving lubrication strategies and predictive modeling, offering valuable insights for enhancing engine performance and durability in automotive engineering.

الملخص البحث

يُعد تقليل الاحتكاك والتآكل بين الأسطح المتلامسة محورًا رئيسيًا في علم الاحتكاك (Tribology) ، خاصة في تحسين أداء زيوت التشحيم لضمان متانة و اعتمادية المحركات. توفر زيوت التشحيم منخفضة اللزوجة فوائد في تحسين كفاءة استهلاك الوقود، لكنها تحديات في تقليل الاحتكاك والتآكل. الانتقال إلى زيوت منخفضة اللزوجة، مثل SAE 5W30 وSAE 0W20، يثير مخاوف بشأن زيادة التلامس السطحي وما قد يترتب عليه من تحديات في المتانة، مما يُبرز الحاجة إلى إضافات متقدمة مثل الجرافين والفوليرين، بالإضافة إلى الطلاءات التي تخفف من هذه المشكلات، مع الاستفادة من تقنيات التعلم الآلي للتنبؤ بالأداء الاحتكاكي وتقليل المحاولات التجريبية المكلفة.لقد اكتسب الجرافين والفوليرين اهتمامًا كإضافات محتملة لتحسين الخصائص الاحتكاكية لزيوت التشحيم. تبحث هذه الدراسة في تأثير إضافة 0.005% وزنيًا من الجرافين والفوليرين إلى زيت التشحيمSAE 0W20 ، بالإضافة إلى ستة أنواع مختلفة من الطلاءاتTiN) ، AlTiN، CrN، TiAlSN، TiCN، و DLC-AlTiN) على كتل فولاذية. الهدف الأساسي هو تطوير مجموعة بيانات تستكشف العلاقة بين هذه الإضافات والطلاءات مع العوامل الاحتكاكية الحرجة، مثل معامل الاحتكاك، مساحة التآكل، ودرجة الحرارة . باستخدام جهاز اختبار الاحتكاك من نوع"Rod and Ring Tribometer" ، تقيس هذه الدراسة الأداء الاحتكاكي، مع إجراء تحليلات SEM و EDXلتوصيف الأسطح. تشير النتائج إلى أن إضافات الجرافين والفوليرين تقلل بشكل كبير من الاحتكاك والتآكل، حيث يُظهر الجرافين قدرة أفضل على تبديد الحرارة. أما الطلاءات، خاصةCrN ، فتُظهر تقليلًا في التآكل والاحتكاك، على الرغم من أن CrN أظهر تآكلاً أعلى مقارنة بالطلاءات الأخرى .تم استخدام نماذج التعلم الآلي، بما في ذلك

الانحدار باستخدام الآلات الداعمة(SVR) ، وغابة القرار العشوائي(RF) ، وشجرة القرار (DT) للتنبؤ بالعوامل الاحتكاكية. وقد تفوقت تقنية RF على SVR و DTفي التنبؤ بكل من الاحتكاك ومساحة التآكل، في حين تميزت DT في التنبؤ بدرجة الحرارة. تسهم هذه الدراسة في تحسين استراتيجيات التشحيم والنمذجة التنبؤية، مما يوفر رؤى قيمة لتعزيز أداء المحركات ومتانتها في هندسة السيارات.

APPROVAL PAGE

I certify that I have supervised and read this study and that in my opinion, it conforms to acceptable standards of scholarly presentation and is fully adequate, in scope and quality, as a dissertation for the degree of Master of Science in Engineering

....
Shafie Kamaruddin
Supervisor

....
Aishah Najiah Dahnel
Co-Supervisor

....
Mohd Hafis Sulaiman
Co-Supervisor

I certify that I have read this study and that in my opinion it conforms to acceptable standards of scholarly presentation and is fully adequate, in scope and quality, as a dissertation for the degree of Master of Science in Engineering.

....
Muhammad Mukhtar Noor Awalludin
Internal Examiner

....
Mohd Ridzuan Mohd Jamir
External Examiner

This dissertation was submitted to the Department of Manufacturing and Materials Engineering and is accepted as a fulfilment of the requirement for the degree of Master of Science in Engineering.

....
Ahmad Zahirani Ahmad Azhar
Head, Department of
Manufacturing and Materials
Engineering

This dissertation was submitted to the Kulliyyah of Engineering and is accepted as a fulfilment of the requirement for the degree of Master of Science in Engineering.

....
Khairul Azami Sidek
Dean, Kulliyyah of Engineering

DECLARATION

I hereby declare that this thesis is the result of my own investigation, except where otherwise stated. I also declare that it has not been previously or concurrently submitted as a whole for any other degrees at IIUM or other institutions.

Muhammad Hazman Sharuddin

Signature .... Date 13 February 2025

INTERNATIONAL ISLAMIC UNIVERSITY MALAYSIA

DECLARATION OF COPYRIGHT AND AFFIRMATION OF FAIR USE OF UNPUBLISHED RESEARCH

PREDICTING TRIBOLOGICAL PERFORMANCE OF LIQUID LUBRICANTS AND COATED-SURFACES BYMACHINE LEARNING APPROACHES

I declare that the copyright holder of this dissertation is jointly owned by the student and IIUM.

No part of this unpublished research may be reproduced, stored in a retrieval system, or transmitted, in any form or by any means, electronic, mechanical, photocopying, recording or otherwise without prior written permission of the copyright holder except as provided below.

1. Any material contained in or derived from this unpublished research may be used by others in their writing with due acknowledgement.

2. IIUM or its library will have the right to make and transmit copies (print or electronic) for institutional and academic purposes.

3. The IIUM library will have the right to make, store in a retrieval system and supply copies of this unpublished research if requested by other universities and research libraries.

By signing this form, I acknowledged that I have read and understand the IIUM Intellectual Property Right and Commercialization policy.

Affirmed by Muhammad Hazman Sharuddin

.... 13 February 2025

Signature Date

This thesis is dedicated to my loving parents, whose support and sacrifices have enabled me to achieve my dreams. To my supervisor, Dr. Shafie, and Co-Supervisor, Dr. Aishah and Ir. Dr. Hafis whose expertise and guidance have been instrumental in shaping this work. And to all my friends and family who believed in me and provided unwavering encouragement throughout this journey. Thank you for being my pillars of strength

ACKNOWLEDGEMENTS

First and foremost, I would like to express my deepest gratitude to my family. Their unwavering support, encouragement, and belief in my abilities have been a constant source of strength throughout this journey. To my parents, thank you for the sacrifices you have made and for always being there for me. Your love and guidance have been instrumental in shaping who I am today.

To my beloved wife, your patience, understanding, and unwavering support have been invaluable. You have been my rock, providing me with the encouragement I needed to persevere through the challenging times. Your love and companionship have been my greatest motivation.

I am also profoundly grateful to my friends, whose companionship and encouragement have made this journey more enjoyable and less daunting. Your constant support, whether through words of encouragement or simply being there when I needed a break, has been greatly appreciated.

I would like to extend my heartfelt thanks to my supervisor, Dr. Shafie and Co-Supervisors, Dr. Aishah and Dr. Hafis. Their expertise, guidance, and patience have been essential in the completion of this thesis. Your insightful feedback and constructive criticism have helped me refine my ideas and improve my research. I am truly blessed with your mentorship and support.

Lastly, I would like to acknowledge everyone who has contributed to this work, directly or indirectly. Your support and encouragement have made this achievement possible.

Thank you all.

TABLE OF CONTENTS

LIST OF TABLES

LIST OF FIGURES

LIST OF ABBREVIATIONS

AISI	American Iron and Steel Institute
SAE	Society of Automotive Engineers
TiN	Titanium Nitride
TiCN	Titanium Carbo-Nitride
AlTiN	Titanium aluminum nitride
CrN	Chromium Nitride
DLC-AlTiN	Diamond like coating Titanium aluminum nitride
TiAlSN	Titanium aluminum Tin
SEM	Scanning electron microscope
EDX	Energy Dispersive X-ray (EDX)
SVR	Support vector regression
DT	Decision tree
RF	Random forest
ML	Machine learning
COF	Coefficient of friction
PVD	Physical Vapor Deposition
HiPIMS	High Power Pulsed Magnetron Sputtering
GO	Graphene oil
FO	Fullerene oil
HRC	Hardness Rockwell C Scale
ASTM	American Society for Testing and Materials
MAE	Mean absolute error
MSE	Mean squared error
RMSE	Root mean squared error

CHAPTER ONE

INTRODUCTION

1.1 BACKGROUND OF STUDY

Tribology is one of the most important fields in today's engineering studies, which plays significant role in our daily life; dental care, cleaning, sports and travelling. Tribology is a science that focuses on understanding, managing and reducing friction and wear through the mean of lubrication (Dhanola et al., 2022). It is always necessary to enjoy modern civilised lifestyle. Modern day equipment such as automotive equipment, heavy machinery, computer devices utilise tribology to function normally. Occasionally, a machine will break down typically caused by failure of moving parts. Lubrication is crucial to extending machine lifespan and increase reliability. A lubricant is a substance that introduced in between moving surfaces to reduce friction wear and heat. Furthermore, lubrication minimise unfavourable vibration and noise generated by moving contacts (Sudeep et al., 2015), lubrication can improve in comfort during operation. Friction and wear between contact surfaces lead to failure of components including gear and bearings is essential for the efficient operation of mechanical systems. In addition, friction and wear lead to loss of energy driving the mechanical system less efficient. The importance of tribology is reflected by the large share of the world energy consumption (Holmberg & Erdemir, 2017). Therefore, it is necessary to develop new technologies to reduce the world energy consumption with the advancement in the tribology field. Energy efficiency of modern petrol and diesel powered engine ranges up to 27 % and 37 % respectively has contributed to the global energy demand (Albatayneh et al., 2020). More efficiency energy use will be achieved by reducing frictional energy losses (Liu & Dumitrescu, 2019).

With new technologies and applications emerging that operate intense conditions, lubricants are required to satisfy the demand. Enhancing the properties of lubricant through various methods is important area of research in the field of research. The development of various lubricating oil additives has been studied by several researchers. To improve the qualities of lubricating oil, a small weight percentage of additives are added to the base oil to improve the tribological performance of lubricants

(Liñeira del Río et al., 2022). Nanotechnology has been adopted in various fields of science. Several studies have demonstrated the effectiveness of adding nanoparticles to lubricant as a method to enhance the lubricant's tribological performance (Oganesova et al., 2018). Frictional losses can be improved by applying antifriction coatings and using additives in lubricants (Lee & Zhmud, 2021).

Recent researchers have successfully integrated ML and AI as reliable tools to predict tribological properties (Hasan et al., 2022). Due to abundance of data on friction and wear behavior, the multiple parameter analysis require data driven approaches especially for complex materials such as two-phase composites whose surface characteristics change over time. Due to the complexities of the many characteristics that determine friction and wear, traditional analysis that focuses on single experimental observations frequently falls short in producing a comprehensive knowledge of tribological behaviour. With the emergence of ML and AI techniques, it has become possible to study and explore new connections in data-driven scientific fields. With the development of ML and AI technologies, it has significantly improved the efficiency of information processing method (Zhang et al., 2021). Modern computing systems are able to use ML and AI algorithms to discover novel correlations in data-driven areas that would be unfeasible using conventional methods. Integrating informatics and tribology have improved the tribological research efficiency. In recent development, AI and ML is used to predict the tribological data which will improve the ability to anticipate and manage the tribological behavior of materials (Rosenkranz et al., 2021).

Limited work has been reported on the tribological performance of graphene and fullerene as lubricating additives, particularly in low-viscosity SAE 0W20 oils with coatings. Despite their promising friction-reducing and wear-resisting properties, challenges such as dispersion stability, compatibility with low-viscosity oils, and high production costs limit their practical application. Additionally, their long-term performance and synergistic effects with coatings under operational conditions remain underexplored, with most studies relying on conventional methods rather than predictive modeling. This study addresses these gaps by systematically investigating the tribological performance of graphene, fullerene, and coatings under SAE 0W20 lubrication, complemented by a supervised ML model for performance prediction and evaluation.

1.2 PROBLEM STATEMENT

Engine lubricant oils primarily function to form protective films on contact surfaces, reducing friction and wear to enhance engine durability. However, the shift to low-viscosity lubricants, such as SAE 5W30 and SAE 0W20, raises concerns about increased contact surface area and potential durability challenges. This underscores the need to explore the efficacy of advanced additives like graphene and fullerene, as well as coatings, in mitigating these issues. Despite their potential, limited studies have examined the effects of these additives on the tribological performance of engine lubricants, necessitating thorough experimental investigations.

However, such investigations are often time-consuming and resource-intensive due to the complexity of the variables involved. Recent advancements in AI and ML offer transformative potential in this field. By leveraging data-driven approaches, AI and ML can efficiently analyze the abundance of friction and wear data, particularly for complex materials like two-phase composites with evolving surface characteristics. These predictive systems not only enhance the understanding of tribological behavior but also uncover novel correlations that traditional methods may overlook. As a result, AI-driven models can provide proactive recommendations to manufacturers, optimizing material selection and engine performance while reducing the need for extensive experimental trials. Integrating informatics with tribology thus represents a significant advancement in addressing the challenges of modern lubrication systems.

1.3 RESEARCH OBJECTIVES

This aims of this study are as follows:

i. To develop a dataset by investigating the effects of liquid lubricants on the coefficient of friction, worn area, and temperature under controlled tribological conditions.
ii. To develop a dataset by investigating the effects of surface coatings on the coefficient of friction, worn area, and temperature under controlled tribological conditions.

iii. To predict and validate the coefficient of friction, worn area, and temperature using machine learning models based on the effects of liquid lubricants and surface coatings.

1.4 SIGNIFICANCE OF RESEARCH

The challenge in engine lubrication is highly significant to this research because it directly impacts the durability, efficiency, and performance of modern engines. With the increasing adoption of low-viscosity lubricants, such as SAE 0W20, to improve fuel efficiency, there is a growing risk of insufficient lubrication, leading to increased friction, wear, and potential engine failure. This study addresses these critical challenges by exploring advanced solutions, including the use of liquid lubricants and surface coatings, to optimize tribological performance. By leveraging machine learning approaches, the study aims to predict and manage these tribological issues effectively, ensuring enhanced engine reliability and longevity in response to evolving automotive requirements.

The outcomes of this study are expected to have several notable implications. Firstly, they can inform manufacturers and engineers about the efficacy of different lubrication strategies in reducing friction and wear, thereby improving engine durability and performance. Secondly, the predictive models developed in this study can serve as practical tools for decision-making, facilitating informed recommendations on material selection and lubricant formulation. Ultimately, this research contributes to advancing the understanding of tribological behavior in engine systems and offers practical solutions to optimize engine reliability and longevity.

1.5 SCOPE OF RESEARCH

This study aims to predict the tribological performance of lubricants and coatings using MLmodels, supported by experimental data to develop a comprehensive dataset. The scope of the study includes four types of lubricants: SAE 5W30, SAE 0W20, SAE 0W20 as a base oil, base oil + 0.005 wt.% graphene, and base oil + 0.005 wt.% fullerene.

Six types of surface coatings are considered: TiN, AlTiN, CrN, TiAlSN, TiCN, and DLC-AlTiN. The tribological performance is assessed based on the coefficient of friction, worn area, and temperature, following the ASTM G77 standard.

The experimental parameters are as follows: a rotating speed of 490 rpm, an initial temperature of 30°C, a constant load of 17.7 N, and a lubricant sample volume of 20 ml. The block sample dimensions are 14 mm in diameter and 14 mm in length, with a coating thickness of 3 µm. These parameters are selected to simulate realistic conditions while maintaining controlled and reproducible testing.

Three machine learning algorithms—DT, SVR, and RF—are utilized to predict the coefficient of friction, worn area, and temperature. These algorithms are chosen for their ability to handle complex, nonlinear relationships and their proven efficacy in analyzing tribological systems in prior studies. The study evaluates the predictive accuracy and reliability of these algorithms, with performance assessed through standard metrics such as RMSE and R^2 values.

1.6 ORGANIZATION OF THE REPORT

This thesis focuses on efforts to enhance the understanding and prediction of tribological performance in lubricants and surface coatings using machine learning approaches. The study integrates experimental investigations with data-driven techniques to address the challenges associated with wear and friction in engine lubrication systems. The chapters are structured to provide a comprehensive exploration of the research objectives, methodologies, and findings.

Chapter 1: Introduction

This chapter provides an overview of the research background, highlighting the significance of tribological challenges in modern engine lubrication. It outlines the research problem, objectives, scope, and limitations, establishing the foundation for subsequent chapters.

Chapter 2: Literature Review

This chapter discusses previous studies on the tribological performance of liquid lubricants and surface coatings, with a particular focus on the role of additives like graphene and fullerene. It also reviews the application of machine learning in tribological research, identifying gaps that this study aims to address.

Chapter 3: Methodology

This chapter details the experimental setup, including the selection of lubricants, coatings, and test parameters as per ASTM G77 standards. It also explains the data collection process and the machine learning techniques used, such as Decision Tree, Support Vector Regression, and Random Forest algorithms.

Chapter 4: Results and Discussion

This chapter presents the findings of the experimental and machine learning analyses. It includes a discussion on the effects of lubricants and coatings on tribological performance and evaluates the predictive accuracy of the machine learning models.

Chapter 5: Conclusion and Recommendations

This chapter summarizes the key findings, discusses their implications for tribological research and practical applications, and provides recommendations for future work.

CHAPTER TWO

LITERATURE REVIEW

2.1 INTRODUCTION

Tribology, the interdisciplinary field focused on the study of friction, wear, and lubrication, has gained considerable attention due to its vital role in enhancing the performance and longevity of mechanical systems. As industries strive to improve efficiency and reduce material degradation, understanding the principles of tribology becomes increasingly essential. This literature review explores the fundamental concepts of tribology, including the mechanisms of friction, various types of wear, and the role of lubricants in minimizing frictional forces. Additionally, it examines the integration of AI and machine learning techniques in tribological research, particularly in predictive modeling and data analysis. These advanced technologies facilitate the identification of wear patterns, optimize lubricant formulations, and enhance the design of tribological systems by enabling more accurate predictions of performance under varying conditions. By synthesizing current knowledge and highlighting the transformative impact of AI and machine learning, this review aims to provide a comprehensive foundation for future research and innovation in the field of tribology.

2.2 TRIBOLOGY

2.2.1 FRICTION

Friction is not an inherent material property but rather a response of the system (Ludema & Ajayi, 2018). It represents the resistance experienced by one object in motion relative to another object with which it is in contact (Hutchings & Shipway, 2017). Figure 2.1 illustrates the movement of the upper part of the body when a force F is applied in both sliding and rolling scenarios. The fundamental laws of friction dictate that the frictional force is perpendicular to the normal load, and neither the contact area nor the sliding speed affects this force (Hutchings & Shipway, 2017). Moreover, according to Hutchings and Shipway (2017), the coefficient of friction varies from low to high, impacting the magnitude of the frictional force. This coefficient, denoted by μ, typically ranges from 0.1 to 1 for materials sliding without lubricants.

The forces of friction can be categorized into two which are dry friction and wet friction (Bhushan, 2013). Force of friction between two surfaces without lubricants is called dry friction while wet friction is force of friction between surfaces in the presence of lubricants. Static friction and kinetic friction are also two groups of friction. Static friction is the friction between two surfaces that are not in motion. Kinetic friction is the friction between surfaces that are moving. Static friction is the force to start an object from a static position to start the motion. Kinetic force is the force that required to keep an object to stay in movement (Bhushan, 2013). The kinetic friction force is usually smaller compared to static friction force, as in Figure 2.2.

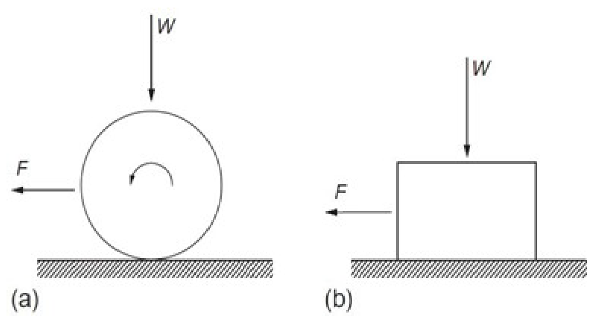

Figure 2.1 Force F is needed to counter friction and induce motion by (a) rolling and (b) sliding (Hutchings & Shipway, 2017).

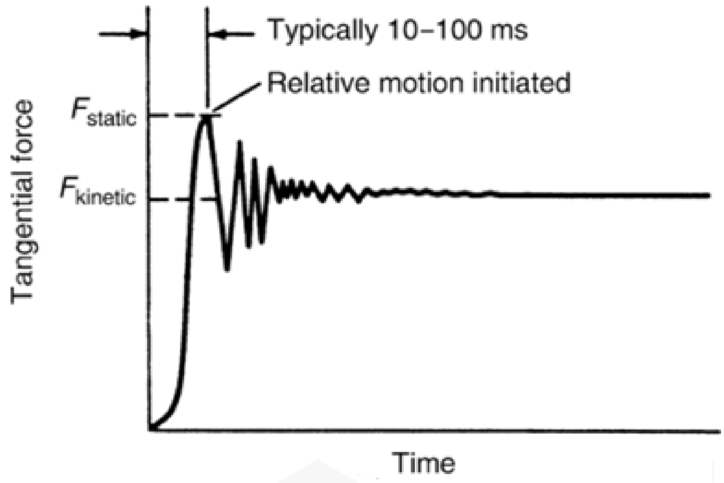

Figure 2.2 Tangential force as function of time (Bhushan, 2013)

2.2.2 WEAR

Wear can be defined as the transfer of material from one surface to another, occurring either within the same body or due to surface damage induced by movement (Almen, 1950). Wear can also be known as loss of materials from the surface as a result of movement on the surface (Stachowiak, 2005). Wear can be caused by purely mechanical, for example brittle fracture or plastic deformation, or may be caused by chemical reactions, for example oxidation of a metal (Stachowiak, 2005).

There are many components that are susceptible to wear everyday such as shoes, brakes, dies, door hinges, engine cams, teeth and joints, and many more (Ludema & Ajayi, 2018). Wear can sometimes be desirable in some situations but most of the time wear can bring negative effects and not is desirable especially in engineering application. Example of desirable wear is when writing using a pencil and the lead of the pencil transfer to paper due to friction between the paper and the pencil lead. Wear is not desirable in machine applications such as cams, gears and bearings (Bhushan, 2013).

There are many types of wear mechanisms such as sliding wear or adhesive wear, abrasive wear, fatigue wear, chemical and corrosive wear (Li & Tsu, 2019). The classification of wear parameters is shown in Table 2.1. Most surfaces that encounter wear are usually because of two or more mechanisms of wear simultaneously (Ludema & Ajayi, 2018).

Table 2.1 Classification of wear parameters (Stachowiak, 2005)

Class	Parameter						
Friction type	Rolling	Rolling–sliding	Sliding	Fretting	Impact		
Contact shape	Sphere/ sphere	Cylinder/ cylinder	Flat/ flat	Sphere/ flat	Cylinder/ flat	Punch/ Flat	
Contact pressure level	Elastic	Elasto-plastic	Plastic				
Sliding speed or loading speed	Low	Medium	High				
Flash temperature	Low	Medium	High				
Mating contact material	Same	Harder	Softer	Compatible	Incompatible		
Environment	Vacuum	Gas	Liquid	Slurry			
Contact cycle	Low (single)	Medium	High				
Contact distance	Short	Medium	Long				
Phase of wear	Solid	Liquid	Gas	Atom	Ion		
Structure of wear particle	Original	Mechanically mixed	Tribochemically formed				
Freedom of wear particle	Free	Trapped	Embedded	Agglomerated			
Unit size of wear	mm scale	µm scale	nm scale				
Elemental physics and chemistry in wear	Physical adsorption, chemical adsorption, tribochemical activation and tribofilm formation, oxidation and delamination, oxidation and dissolution, oxidation and gas formation, phase transition, recrystallization, crack nucleation and propagation, adhesive transfer and retransfer						
Elemental system dynamics related to wear	Vertical vibration	Horizontal vibration	Self-excited vibration	Harmonic vibration	Stick-slip motion		
Dominant wear process	Fracture (ductile or brittle)	Plastic flow	Melt flow	Dissolution	Oxidation	Evaporation	
Wear mode	Abrasive	Adhesive	Flow	Fatigue	Corrosive	Melt	Diffusive
Wear type	Mechanical	Chemical	Thermal				

2.2.2.1 Sliding Wear

Sliding wear occurs when two surfaces move against each other, commonly referred to as adhesive wear (Hutchings & Shipway, 2017). This type of wear results in a reduction in the volume of material on the surfaces as they slide against each other. Figure 2.3 shows an example of sliding wear that occurs on AISI 304 stainless steel shaft observed using scanning electron microscope (SEM). Sliding wear also caused separation of materials due to adhesion on the surface and transfer of the materials from the original surface to secondary surface (Bhushan, 2013). When sliding happens some of the materials might come off the original materials and become debris. Some materials are during recurrent loading and unloading action resulting in fatigue that leads to formation of loose debris.

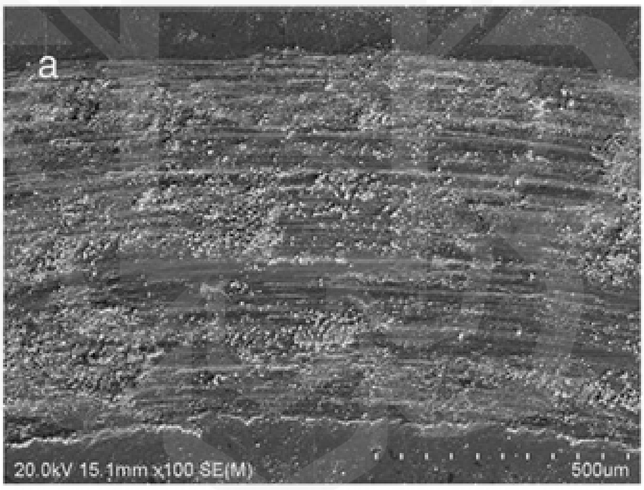

Figure 2.3 Sliding wear of AISI 304 stainless steel observed under SEM (Jin et al., 2013)

According to Hutchings and Shipway (2017), when the surfaces are sliding with the presence of lubrication, the wear will be known as lubricated sliding wear. For sliding surfaces that operate without lubricants, the wear that happens is called dry sliding wear (Aydin & Durgut, 2021). Lubricated wear can be categorized into two, well-lubricated wear systems and marginally lubricated wear systems (Stachowiak, 2005). Well lubricated wear system can obtain a very small coefficient of wear value of *K* of around 10-8 to 10-12 and the chemical additives help to control the rate of wear on the surfaces and enable the surfaces to withstand a higher load for a longer period of time (Stachowiak, 2005). A marginally lubricated wear system usually uses a non-reactive lubricant and commonly will have a higher *K* value compared to the well-lubricated system (Stachowiak, 2005).

MLhas shown promise in predicting sliding wear behavior in tribological systems, especially under conditions involving liquid lubricants and coated surfaces (Rajput & Das, 2023). Sliding wear, a critical factor in the performance of moving components, depends on complex interactions between lubricant properties, surface coatings, and operating conditions such as load and sliding velocity. Studies integrating ML models with experimental tribological data have demonstrated the ability to accurately predict wear rates, coefficient of friction, and temperature rise (Rajput & Das, 2023). By leveraging algorithms like support vector machines and random forests, these approaches provide a robust framework for optimizing lubricant formulations and coating materials, addressing critical challenges in reducing wear and improving system durability.

2.2.2.2 Adhesive Wear

Adhesive wear occurs when two surfaces in contact experience localized bonding due to intermolecular forces as shown in Figure 2.4. This type of wear is particularly significant in metal-to-metal contacts, where the adhesion can lead to material transfer from one surface to another. During operation, especially under high loads or pressures, small areas of contact may bond, and when these bonds break, they can result in the loss of material, creating wear debris. Studies have shown that factors such as surface roughness, hardness, and the presence of lubricants play a crucial role in determining the extent of adhesive wear (Yadav et al., 2023) . Effective lubrication can reduce the direct contact between surfaces, minimizing adhesion and, consequently, wear. Recent research has focused on surface treatments and coatings that enhance wear resistance by altering the surface properties, thereby reducing adhesive wear in critical applications like gears and bearings.

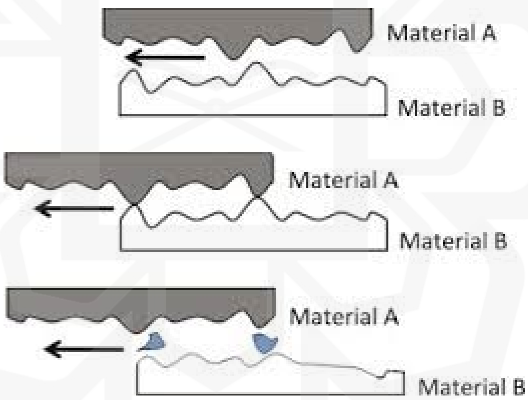

Figure 2.4 Adhesive wear (Yadav et al., 2023)

2.2.2.3 Abrasive Wear

Abrasive wear, on the other hand, occurs when hard particles or rough surfaces scrape against a softer material, leading to material removal as shown in Figure 2.5. This phenomenon is commonly seen in environments where contaminants like dust or grit are present, significantly affecting the performance and lifespan of machinery. Abrasive wear can be classified into two main types: two-body and three-body wear. In two-body abrasive wear, two solid surfaces are in direct contact, while in three-body abrasive wear, a third body (such as particles) is introduced into the contact area, increasing the potential for material loss. The severity of abrasive wear depends on factors such as the hardness of the materials involved, the size and shape of the abrasive particles, and the applied load (Shen et al., 2018). Advances in material science have led to the development of harder and more resilient materials, as well as improved coatings designed to withstand abrasive conditions. Understanding these wear mechanisms is essential for designing more durable components in industries like mining, construction, and manufacturing.

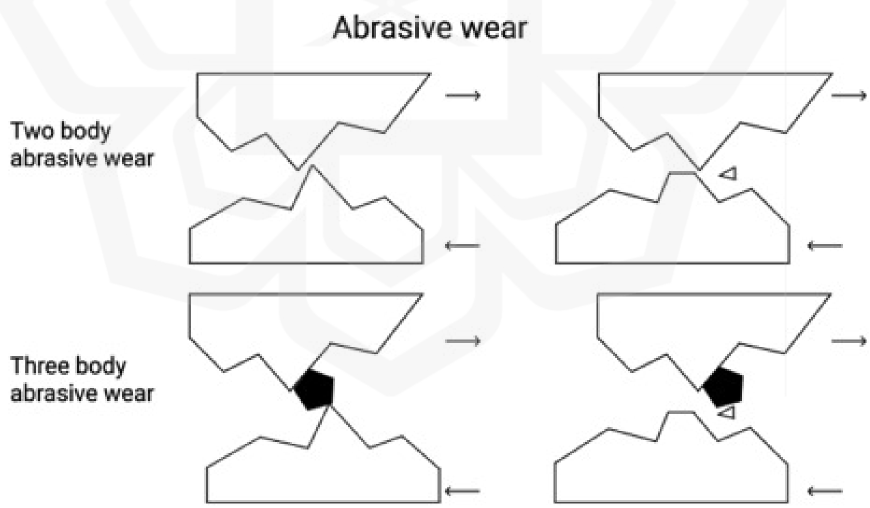

Figure 2.5 Abrasive wear (Shen et al., 2018)

2.3 LUBRICANTS AND LUBRICATIONS

Lubrication involves applying a substance to enhance the smoothness of motion between two surfaces, typically referred to as a lubricant. According to Lansdown (2004), lubricants can come in many forms such as liquids, semi-liquids, solids, gasses or any combinations of solids, liquids and gasses. Lubrication can help to reduce friction and wear on surfaces (Bhushan, 2013). A lubricant function by introducing a layer of film between the sliding surfaces that help to reduce the frictional force between surfaces and thus helping to reduce the rate of sliding wear (Ghalme et al., 2020).

Lubricants usually are divided into four different classes which are oils, greases, dry lubricants and gasses (Lansdown, 2004). Because there are so many lubricants that are available from different manufacturers, the problem of selection of lubricant arises. Selecting the right lubricants to use based on the application is important to prevent problems such as high lubricant consumption, leakage or short lubrication life (Lansdown, 2004). The properties of different lubricant types can be seen in Table 2.2.

When choosing a lubricant, two primary factors often considered are the speed and load (Xie & Zhu, 2021). Figure 2.4 shows the speed at bearing contacts and load limits for different types of lubricant. For example, the maximum specific load for plain soft grease is around 2000 kN/m2 while the maximum specific load for an extreme pressure grease is around 7000 kN/m2. Based on the figure, oil is quite flexible since it covers a wide range of speed and load making it a common choice of lubricant for car engines and transmission fluids (Kamel et al., 2020).

Table 2.2 Properties of basic lubricant types (Lansdown, 2004)

Lubricant property	Oil	Grease	Dry lubricant	Gas
1. Hydrodynamic lubrication	Excellent	Fair	Nil	Good
2. Boundary lubrication	Poor to excellent	Good to excellent	Good to excellent	Usually poor
3. Cooling	Very good	Poor	Nil	Fair
4. Low friction	Fair to good	Fair	Poor to good	Excellent
5. Ease of feed to bearing	Good	Fair	Poor	Good
6. Ability to remain in bearing	Poor	Good	Very good	Very poor
7. Ability to seal out contaminant	Poor	Very good	Fair to good	Very poor
8. Protection against atmospheric corrosion	Fair to excellent	Good to excellent	Poor to fair	Poor to good
9. Temperature range	Fair to excellent	Good	Good to excellent	Excellent
10. Volatility	Very high to low	Generally low	Low	Very high
11. Flammability	Very high to very low	Generally low	Generally low	Unlimited variation
12. Compatibility	Very bad to good	Fair to good	Excellent	Generally good
13. Cost of lubricant	Low to very high	Fairly high to very high	Fairly high	Generally very low
14. Complexity of bearing design	Fairly low	Fairly low	Low to high	Very high
15. Life determined by	Deterioration and contamination	Deterioration	Wear	Ability to maintain gas supply

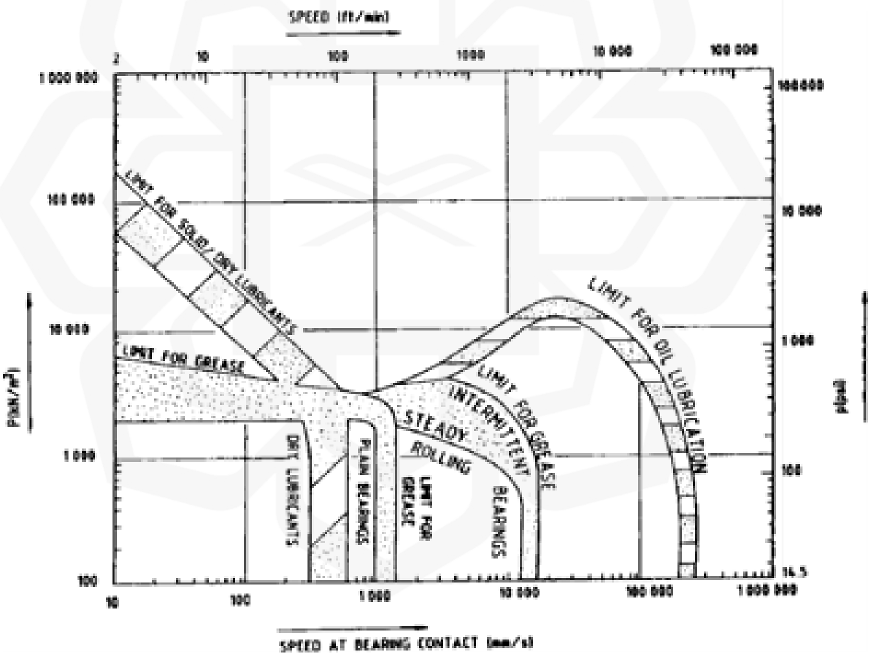

Figure 2.6 Speed and load limits for different lubricant (Lansdown, 2004)

2.4 COATINGS

A coating refers to a deposited layer of substance applied onto a surface to impart advantageous properties (Richard, 2013). The earliest ways to deposit coatings of metal on the surface of another part is by using electroplating and till now the method is still widely used in the industry (Łępicka et al., 2020). However, since the advancement of technology, the methods to depositing coatings on the surface has been varied and coatings can be deposited in the form of liquid, vapour or even solid (Hutchings & Shipway, 2017).

Coatings can be applied directly into the surface of the components without changing the current design since most coatings thickness is less than the components dimensional tolerances (Ludema & Ajayi, 2018). Coatings thicknesses usually vary from a few hundred nanometers up to a few hundred micrometers depending on their intended applications. Coatings play a crucial role in mitigating friction and wear in metal-to-metal contact scenarios. Additionally, they enhance surface hardness, bolster thermal stability, enabling surfaces to endure higher temperatures, and augment chemical stability (Pusch et al., 2011).

Lubrication entails the application of a substance to improve the smooth movement of one surface over another, commonly known as a lubricant. According to Lansdown (2004), lubricants can exist in various forms, including liquids, semi-liquids, solids, gases, or any combination thereof. Lubrication serves to diminish friction and wear on surfaces (Bhushan, 2013). A lubricant operates by establishing a film layer between the sliding surfaces, thereby reducing frictional forces and consequently minimizing the rate of sliding wear (Özkan et al., 2018).

2.4.1 Physical Vapor Deposition (PVD)

PVD process is the process whichmaterials are turn into vapour and deposited on the surfaces in a vacuum or low-pressure plasma environment which can be used to produce thin coatings and films (Mattox, 2010). In PVD the materials change from condensed phase to the vapour phase and return to the original condensed phase so that it can adhere to the surface of part or components (Singh et al., 2019). Titanium Nitride (TiN) coating is one of the earliest PVD coating that was being produced and was used for drilling and milling operation in the past (Inspektor & Salvador, 2014).

Two of the most common PVD techniques are sputtering and evaporation. Due to rapid advancement of technology and science, many new techniques of coating application are introduced into the market (Srinath & Prasad, 2020). Figure 2.5 shows some of the PVD processing techniques. There are also hybrid coatings which allow the usage of different of coatings techniques for specialized applications that required a mixture of properties from various types of coating materials.

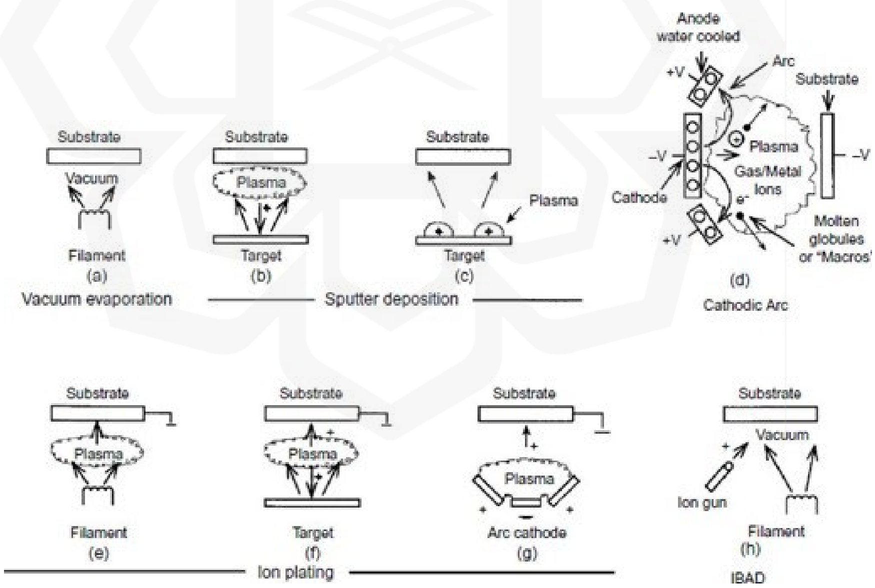

Figure 2.7 PVD Processing Techniques (Mattox, 2010)

2.4.2 High Power Pulsed Magnetron Sputtering (HiPIMS)

HiPIMS is the one of the sputtering techniques under PVD which uses a high voltage pulsed power source to deposit coatings film on the surfaces. Vladimir V. Kouznetsov was the person that patterned the technology in the year 1999 and the technology has gain attention from researcher and industry since HiPIMS can produce harder, denser and smoother coatings with virtually no droplets compared to other coating techniques (Mattox, 2010). Magnetic fields which were used in this technique help to intensify the sputtering process and allow the electron to move along cycloid motion and allows higher ionization yield compared to conventional sputtering process (Gee et al., 2014). Figure 2.6 shows picture of the HiPIMS process.

It is an advanced Physical Vapor Deposition (PVD) technique that employs high-voltage, high-power pulses to generate a dense plasma for depositing thin films. Unlike conventional magnetron sputtering, HiPIMS delivers power in short, intense bursts, resulting in a highly ionized sputtered flux. This ionization enhances the energy and reactivity of the coating species, leading to superior film properties such as improved adhesion, higher density, and better uniformity. The process is widely recognized for its ability to deposit coatings with exceptional hardness, wear resistance, and corrosion protection, making it ideal for applications in tribology, optics, and electronics.

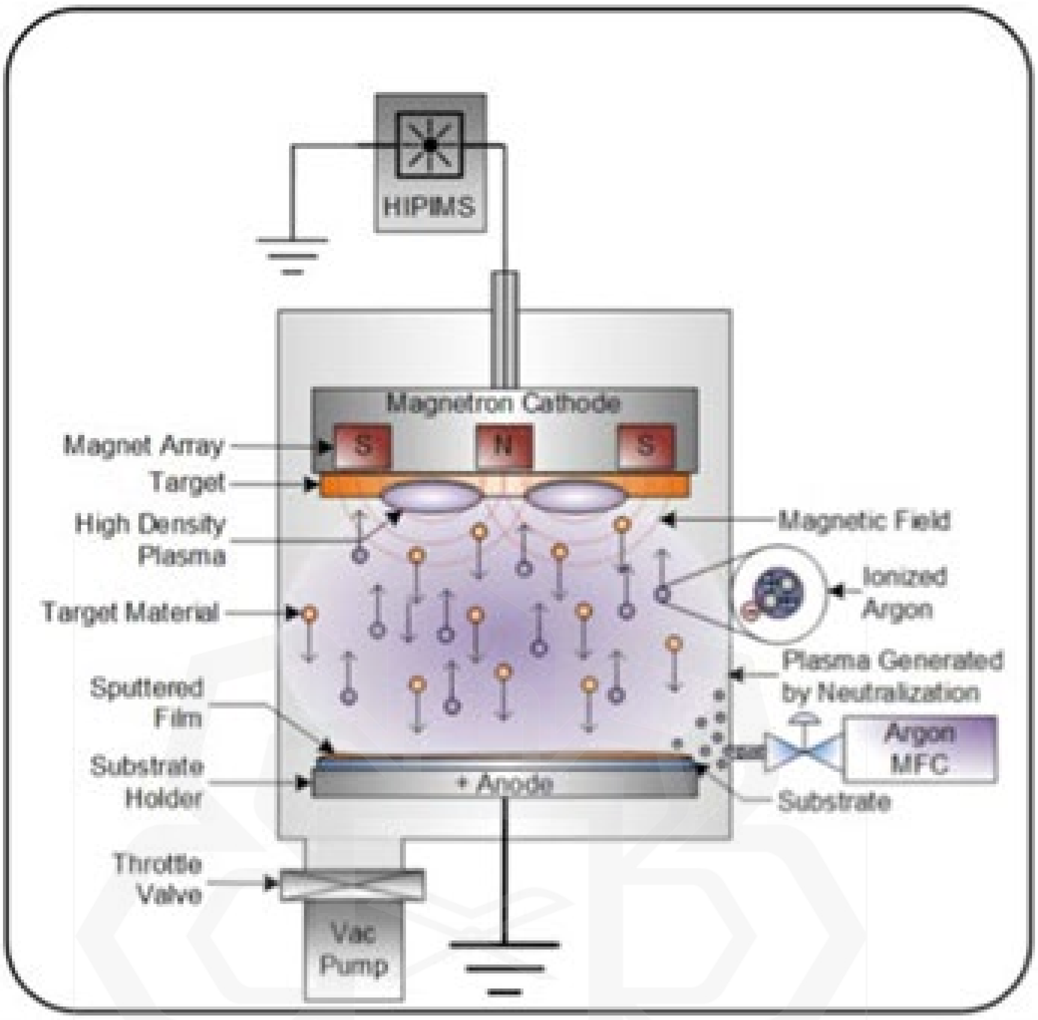

Figure 2.8 Diagram of the HiPIMS Process (Matt, 2016)

2.5 BLOCK ON RING TEST

The block on ring (ASTM G77) test is extensively utilized as a sliding wear assessment method to evaluate the wear characteristics of materials across various conditions and environments (La et al., 2020). Parameters such as normal loading, friction, speed, and lubrication exert significant influence on the wear properties of materials. This tribometer serves as a valuable tool for assessing coatings, lubricants, greases, additives, and sliding performance. Figure 2.7 provides a schematic representation of the contact geometry between the block and the ring. The COF is measured in real-time using load cells, while wear is quantified through weight loss or the dimensions of the wear scar observed using optical microscopy or advanced imaging tools like SEM. Lubricants and coatings are often evaluated to assess their effectiveness in reducing wear and friction. For instance, coatings like CrN, TiAlN, and DLC demonstrate reduced wear volume compared to uncoated materials under similar conditions, highlighting their ability to enhance durability in sliding applications (Ideris et al., 2023). The test is required for understanding wear mechanisms such as adhesive, abrasive, or oxidative wear and for optimizing lubrication strategies, particularly with advanced formulations such as nano-additive lubricants (Rui et al., 2023).

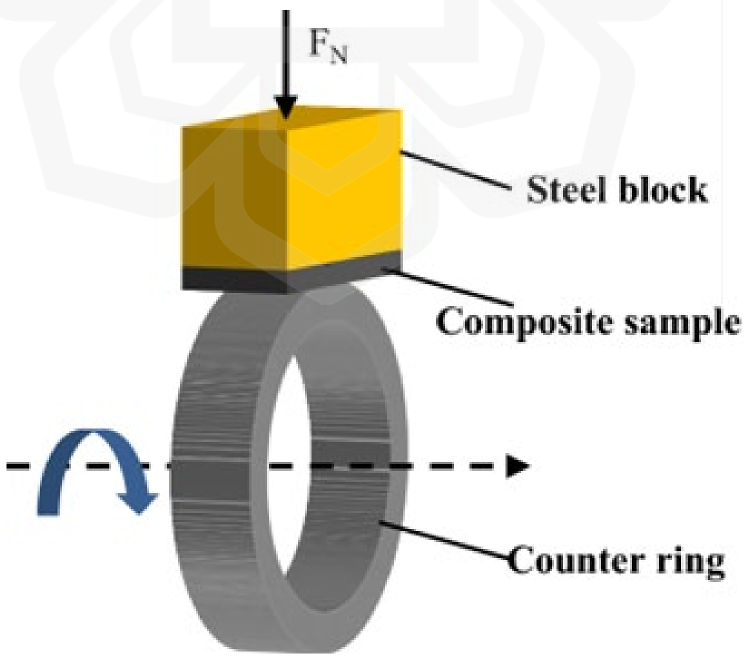

Figure 2.9 Schematic view of block on ring test (Tong et al., 2019)

2.6 ARTIFICIAL INTELLEGENCE (AI) IN TRIBOLOGY

In the expansive realm of AI, machine learning represents a subset focused on cultivating intelligence through experiential learning. According to Das et al. (2015), machine learning is defined as the field of study that enables computers to learn autonomously without explicit programming. Similar to human problem-solving approaches, AI systems are employed to tackle complex tasks. Traditional machine learning methods are typically categorized into supervised learning, unsupervised learning, and reinforcement learning, as illustrated in the tree map depicted in Figure 2.10 by Hasan et al. (2022).

The application of AI in tribology represents a transformative shift in understanding and predicting wear and friction behaviors. AI facilitates the analysis of complex tribological systems by processing vast datasets that encompass variables such as material properties, operating conditions, and environmental factors. Through machine learning algorithms, such as SVM, RF, and ANN, AI can model nonlinear interactions, identify patterns, and predict outcomes with significant accuracy (Marian et al., 2021). For instance, these tools have been employed to predict the wear rates of materials under various lubricating conditions and to optimize surface coatings for enhanced durability. By integrating AI, researchers can significantly reduce experimental time and resources, while also gaining deeper insights into the underlying mechanisms governing tribological phenomena (Rosenkranz et al., 2020). This approach not only advances fundamental research but also aids industries in designing more efficient, reliable, and sustainable systems.

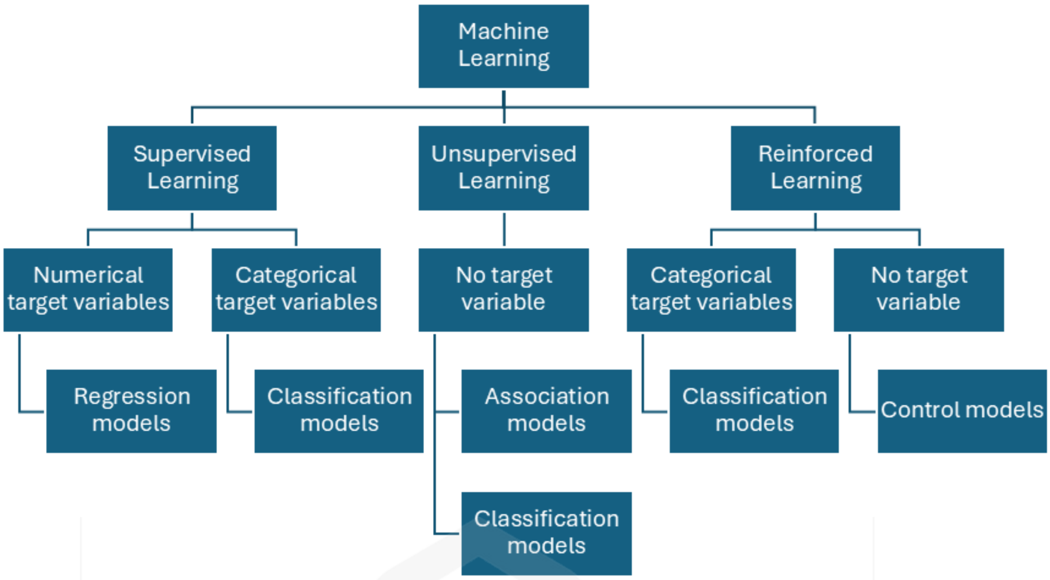

Figure 2.10 Classification of Machine Learning (Hasan et al., 2022)

2.7 TYPES OF MACHINE LEARNING

This section discusses the supervised and unsupervised learning subtypes of machine learning. A wide categorization of ML techniques is presented in Figure 2.11 from a literature study conducted by Rosenkranz et al. (2021). Learning algorithms are being used to understand ever-larger data sets in the engineering industry. In reference to an article written by Das (2015), supervised learning is the process of learning that is based on comparing calculated output and expected output; learning here refers to computing the error and modifying the error for obtaining the intended output. Text recognition and face identification are two of the most well known supervised learning applications. When it comes to data mining, supervised learning may be divided into two categories of concerns which are classification and regression To effectively categorize test data into different groups, classification issues need an algorithm, such as distinguishing spam email in a distinct folder from your inbox. Most often used classification methods are SVM and discriminant analysis.

Regression is another supervised learning method that utilizes an algorithm to understand the relationship between dependent and independent variables. These models are valuable for predicting numerical values using various data inputs, such as estimating sales revenue for a specific company. Linear regression and random forest are examples of common regression techniques.

In contrast, unsupervised learning is a subset of machine learning in which the algorithms are given raw data without labels or clear instructions on how to use it. The learning algorithm should be able to recognise structure on its own in the supplied data. Clustering and dimensionality reduction are the two basic unsupervised learning-based tasks. In contrast to dimensionality reduction, which is a learning method used when a dataset has an excessive amount of features (or dimensions), clustering is a data mining strategy for categorizing unlabeled data into groups based on their similarities or differences (Alloghani et al., 2020). A popular example of clustering is targeted marketing, whereas structure discovery is one of the applications in dimensionality reduction.

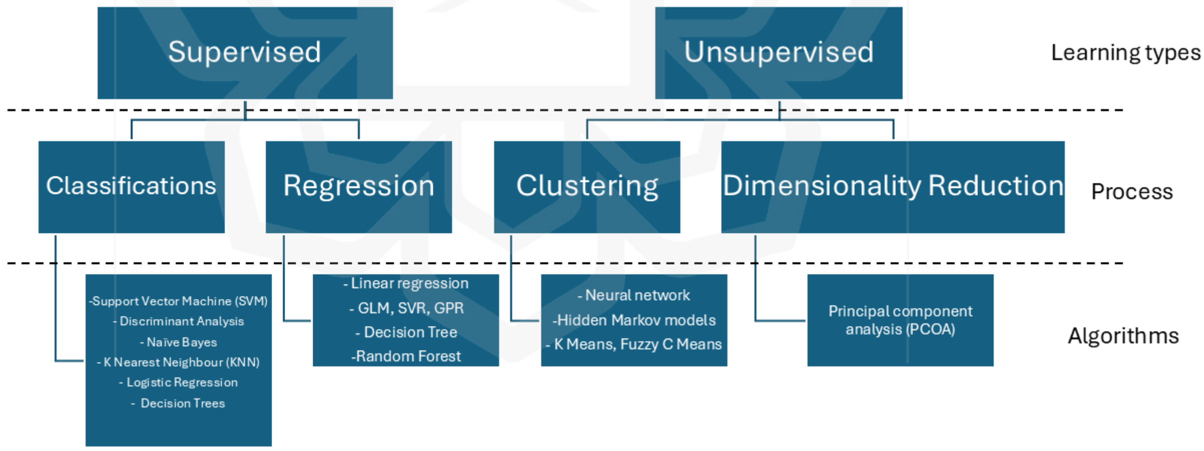

Figure 2.11 Broad Classification of Machine Learning Methods (Rosenkranz et al. (2021)

2.7.1 Support Vector Regression (SVR)

Support Vector Regression (SVR) emerges as a valuable tool in the realm of machine learning, facilitating the prediction of numerical values (Hasan et al., 2022). Operating akin to an astute guide, SVR scrutinizes data points plotted on a graph and constructs a line or curve in close proximity to them. It exhibits a degree of flexibility, akin to a safety zone, by allowing certain deviations from the ideal fit. Unlike rigid approaches, SVR accommodates slight deviations from the line of best fit.

The methodology of SVR involves delineating a line that closely adheres to most data points while permitting a margin of flexibility. This adaptive approach acknowledges that not all data points need to precisely align with the regression line. Notably, SVR prioritizes pivotal data points referred to as "support vectors," ensuring their significant influence on determining the optimal placement of the regression line.

In essence, SVR facilitates accurate predictions even in scenarios where data deviates from a linear pattern. Its adaptive nature proves invaluable in navigating complexities inherent in the dataset, enabling robust prediction outcomes.

2.7.2 Decision Tree (DT)

Decision tree regression is a machine learning technique designed to predict numerical values. Imagine it as a decision-making flowchart where each step asks a question about the input data, leading to a final prediction. The structure includes a root node starting with the entire dataset, internal nodes posing questions about features, and leaves holding the predicted numerical values. During training, the decision tree learns from known input-output pairs, making decisions by recursively splitting data based on features. In the prediction phase, given new input, the tree navigates through branches based on feature values to reach a leaf, which provides the predicted numerical outcome.

For example, in forecasting house prices, questions like "Is the house size greater than 1500 square feet?" guide the process until a leaf predicts, say, a price of $300,000. DT regression is valuable for capturing intricate relationships in data, but careful consideration is needed to prevent overfitting and optimize performance. It serves as a versatile tool in machine learning, particularly when predicting continuous outcomes is the objective.

2.7.3 Random Forest (RF)

Random Forest is like a smart team of decision-makers in the world of machine learning. Instead of relying on just one DT, it uses a bunch of them, and then their opinions are averaged to make a better prediction. This makes Random Forest really good at handling big sets of data and lots of different factors.

Imagine each DT as a different person in the team. They each have their own strengths and weaknesses, but by working together, they can come up with more accurate predictions. This teamwork also helps avoid a common problem called overfitting, where the model gets too fixated on the training data.To make sure Random Forest performs at its best, we need to tweak two things: the number of features it looks at (max_features) and the number of DTs in the team (n_estimators). Getting these just right is the key to making Random Forest shine.

2.8 APPLYING MACHINE LEARNING IN TRIBOLOGY

2.8.1 Coefficient of Friction (COF)

In tribology, the COF is an important metric for calculating the benefits and drawbacks of tribological parts. Accurate COF forecasts can be achieved, which can be utilised to both analyze the tribological system's future functional condition as well as to direct the choice of pre-preparation operations. The key to improving tribological performance still lies in comprehending tribological behaviour and the impact of various material and tribological factors. In reference to the article written by Hasan et al. (2022), friction is measured using the COF, a dimensionless scalar variable. The following equation represents COF which is the ratio of the normal load (N) pushing the sliding surfaces apart to the friction force (F_f) pushing them together.

$$\mu = F_f / N \qquad (1)$$

According to Bowden and Tabor, adhesion (F_a) and deformation (F_d) are two separate sources of friction for sliding contacts. The whole friction force (F_f) and the COF is frequently expressed as a sum, despite the simplification that these parts are independent.

$$\mu = F_f / N = (F_a + F_d)/N = F_a/N + F_d/N = \mu_a + \mu_d \qquad (2)$$

The COF caused by adhesion and deformation are represented by μ_a and μ_d, respectively. Under various loading situations, adhesion is caused by physical and chemical interactions brought on by molecular forces at the actual area of contact between the surfaces' asperities. Asperities on the mating surfaces, which occur at both the microscopic and macroscopic levels, deform (elastically and plastically), and this is what contributes to friction. For instance, Hasan et al. (2022) conducted an experiment on the yield strength and hardness of aluminium alloys. The most prevalent wear mechanisms discovered in aluminium alloys are melt lubrication wear, adhesive wear, delamination wear, and oxidation-dominated wear. A thin, chemically inert oxide layer form on the surface of aluminium as a result of the frictional heat produced during sliding. Adhesion between the surfaces causes adhesive wear with higher stresses, where the adhesive junctions bend plastically and material is removed from the aluminium surface, including the oxide layer. Metal is plastically sheared in a sliding direction during delamination wear. The subsurface breaking that occurs at specific depths under the surface is what causes the laminate wear particles to form.

Experimental tribological data can be utilized to train ML algorithms for predicting tribological behavior, including the COF, for different material and tribological variable combinations. Advanced ML techniques, such as SVM and ANN, have the capability to identify patterns in the data and adjust their learning process accordingly to provide accurate predictions. This approach can provide a more comprehensive understanding of tribological behavior. In recent years, considerable attention has been devoted to the application of ML algorithms in predicting the COF in various materials, particularly in tribological studies (Hasan et al., 2022b). The ability of ML models to analyze complex datasets has proven invaluable in understanding how material properties, processing parameters, and tribological conditions interact to influence friction behavior.

Studies have demonstrated that features such as hardness, yield strength, and processing techniques significantly affect COF. For example, *K-Nearest Neighbors (KNN)* and *RF* algorithms have been employed to correlate material attributes with frictional outcomes, showcasing their effectiveness in predictive accuracy (Hasan et al., 2022a). Research findings indicate that variables such as normal load and sliding speed are critical in determining COF, with certain models like *Gradient Boosting Machines (GBM)* exhibiting superior performance in capturing these relationships. This growing body of literature underscores the potential of ML techniques to enhance predictive capabilities in tribological performance assessment.

2.8.2 Temperature

Knowledge of the amount of heat produced, the resulting temperature increase and the distribution of that heat in the conduction medium is desirable and frequently necessary in many industrial processes as well as tribological applications. In diverse manufacturing processes and tribological applications, a number of methods have been developed over time for measuring heat and temperatures. They included employing ML to determine the temperature of materials after they had undergone tribology.

According to Kennedy (1984), higher surface temperatures in tribological applications, such as during the sliding motion of two contact surfaces, can lead to various detrimental effects. These effects include oxidation and wear, surface melting, thermoelastic instabilities in the contact zone, degradation of solid or boundary lubrication films, exposure of virgin surfaces leading to adhesion and galling between contact surfaces, and potential ignition of condensates. This highlights how tribology contributes to the elevation of material temperatures, consequently increasing wear rates and worn areas. ML is recognized as one of the approaches to predict and estimate the temperature rise in such scenarios.

2.8.3 Wear Area

Machine learning's application in tribology, particularly for wear volume loss, is a burgeoning area of interest. Traditional wear studies often rely on experimental and analytical methods, which may have limitations in capturing the complexity of tribological processes. Machine learning, utilizing algorithms like neural networks and DTs, offers a promising approach to analyze extensive datasets from wear experiments.

This technology's advantage lies in uncovering intricate patterns within datasets that may challenge conventional methods. By incorporating diverse input parameters like material properties and operating conditions, machine learning enables the development of precise predictive models for wear volume loss under various scenarios.

This approach enhances understanding by identifying hidden correlations and non-linear dependencies between tribological variables, contributing to more comprehensive insights into wear mechanisms. Applications of machine learning in predicting wear volume loss span industries, such as automotive and aerospace, offering informed decision-making on material selection, lubrication strategies, and maintenance schedules to mitigate wear-related issues. The prediction of wear rates in materials through machine learning models has gained traction as a vital aspect of tribology research (Marian et al., 2021). Recent investigations reveal that various ML algorithms, including SVM and ANN, can effectively correlate wear rates with mechanical and tribological parameters (Jia et al., 2024). Factors such as material hardness, sliding distance, and load conditions have been identified as key influencers of wear behavior. For instance, RF has emerged as a particularly robust tool for wear rate predictions, outperforming other algorithms by accurately modeling the intricate relationships among input variables (Pasha et al., 2024). Feature importance analysis further elucidates the predominant role of normal load and hardness in wear performance, thereby guiding the optimization of material selection and processing methods. This evidence emphasizes the importance of leveraging ML methodologies to deepen our understanding of wear mechanisms and to improve the longevity and reliability of engineering materials under operational conditions.

In conclusion, the integration of machine learning in tribology, specifically for wear volume loss, represents a significant advancement. This computational approach holds promise for optimizing materials, reducing maintenance costs, and improving the reliability of mechanical components. Ongoing research is expected to contribute significantly to predictive maintenance and materials science.

2.9 SUMMARY

This chapter examines critical factors that influence friction and wear, including material properties and lubrication, emphasizing their role in tribological performance. The ASTM G77 testing method, recognized for its reliability in assessing friction and wear under sliding conditions, is discussed to highlight its applicability in tribological research. Furthermore, the chapter explores the integration of machine learning algorithms to predict key parameters such as wear, coefficient of friction, and temperature. This approach offers a significant shift from conventional experimental methods, aiming to streamline the analysis and enhance the precision of tribological investigations. The combination of experimental standards and data-driven techniques serves to deepen understanding and improve the efficiency of tribological systems.

CHAPTER THREE

MATERIALS AND METHODOLOGY

This chapter explains the process of the experiment. In this chapter, all the machines and equipment used for the experiment are described. The experiment setup for collecting the data is presented in this chapter. Furthermore, the procedures used for prediction the tribological performance is described in this chapter.

3.1 FLOWCHART OF THE STUDY

Flowchart in Figure 3.1 shows the methodology used in this study. It begins with selecting four types of lubricants namely 0W20, 5W30, GO and FO which were analysed for tribological performance. The selection of lubricants in this study—SAE 0W20, SAE 5W20, graphene-infused oil, and fullerene-infused oil—was driven by their popularity and proven performance in automotive and industrial applications. SAE 0W20 and SAE 5W20 are low-viscosity oils commonly used in modern engines for their ability to improve fuel efficiency and cold-start performance (Ideris et al., 2023). These oils are particularly effective in reducing friction during engine warm-up, thereby enhancing fuel economy without compromising lubrication at higher operating temperature have gained attention in recent years due to their potential to enhance lubrication properties, particularly in terms of wear resistance and thermal stability. Graphene, a nanomaterial known for its high mechanical strength and superior lubrication properties, has been shown to reduce friction and wear in engine systems, contributing to improved durability and performance .

Tribological properties of uncoated bearing steel were analysed using Rod and Ring Tribometer at 490RPM, 17.7N load with sliding distance up to 900m. The wear surface was analysed with Scanning Electron Microscopy and Energy Dispersive X-Ray Parameters such as Coefficient of Friction, wear area and contact surface temperature were measured. The best lubricant is selected based on tribological perfromance.

All the experimental data of both coated and uncoated bearing steel were recorded in data sheet. Machine learning model namely SVR, DT and RF were utilised to predict the COF, temperature and wear area. SVR, DT, and RF were selected for their proven ability to model nonlinear tribological data effectively. Compared to methods like neural networks, they offer better interpretability (DT, RF) and efficiency (SVR), while RF provides enhanced accuracy through ensemble learning, making them ideal for this study. 75% of the data were used to train the Machine learning models and the remaining 25% was used to evaluate the Machine learning models. The predicted data was compared to the actual data. The performance of Machine learning was evaluated based on the accuracy in predicting the COF, temperature and wear area.

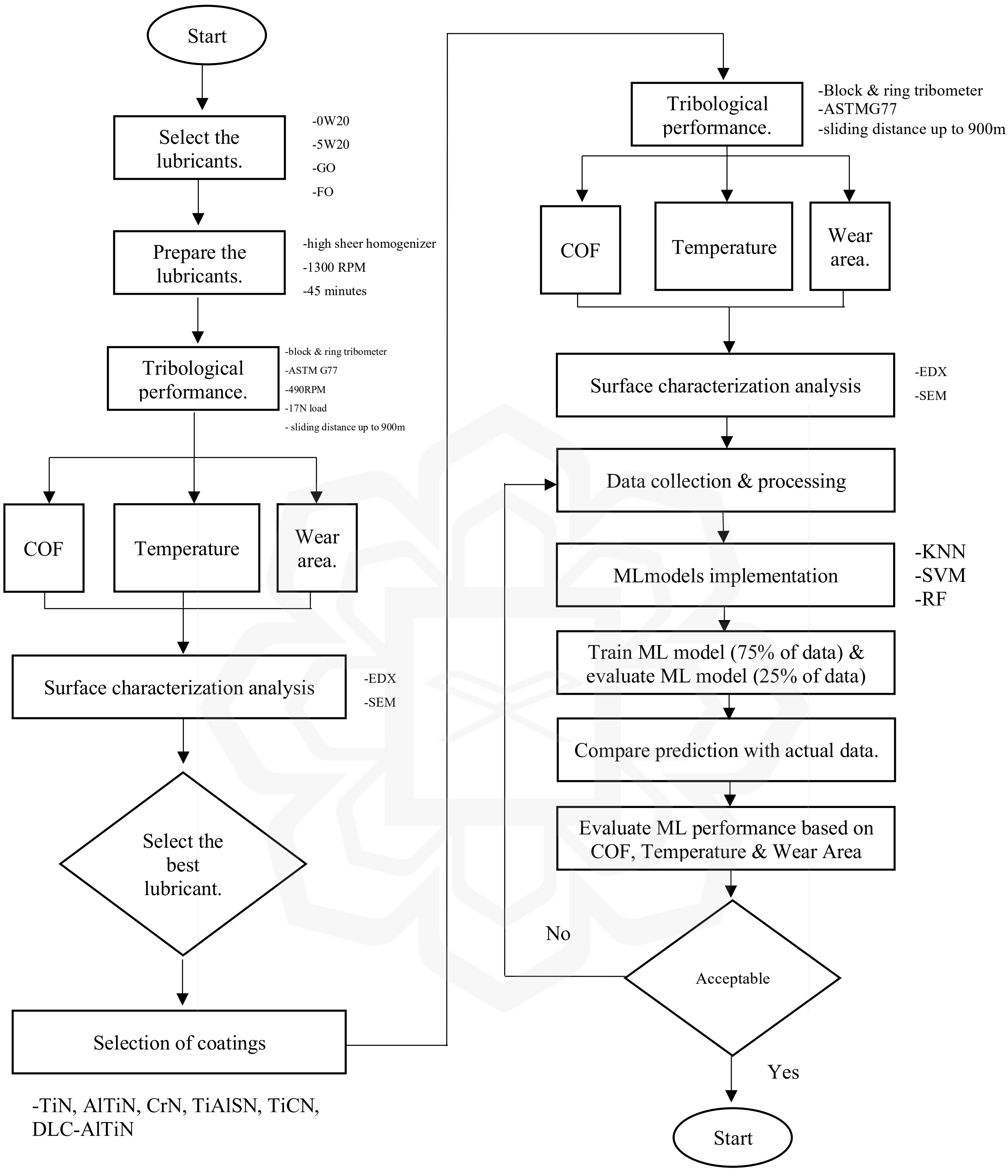

Figure 3.1 Flowchart of the study

The lubricant that produce less wear was used to analysed the performance of coatings. Tribological properties of coatings were analysed using Rod and Ring Tribometer at 490RPM, 17.7N load with sliding distance up to 900m were chosen to reflect moderate sliding conditions representative of real-world applications while maintaining compatibility with ASTM G77 guidelines for wear testing. These values ensure sufficient stress and sliding to evaluate coating performance without introducing extreme conditions that may skew the results. Parameters such as Coefficient of Friction, wear area and contact surface temperature are also evaluated. The coating wear surface was analysed with Scanning Electron Microscopy and Energy Dispersive X-Ray Spectroscopy to identify elemental composition on the wear surface.

All the experimental data of both coated and uncoated bearing stell were recorded in data sheet. Machine learning model namely SVR, DT and RF were utilised to predict the COF, temperature and wear area. SVR, DT, and RF were selected for their proven ability to model nonlinear tribological data effectively. Compared to methods like neural networks, they offer better interpretability (DT, RF) and efficiency (SVR), while RF provides enhanced accuracy through ensemble learning, making them ideal for this study. 75% of the data were used to train the Machine learning models and the remaining 25% was used to evaluate the Machine learning models. The predicted data was compared to the actual data. The performance of Machine learning was evaluated based on the accuracy in predicting the COF, temperature and wear area.

3.2 MATERIALS AND EQUIPMENTS

3.2.1 Block on Ring Test Machine

The study on the tribological performance of the test oils included a durability test, illustrated in Figure 3.2. Bearing steels were utilized to evaluate the tribological characteristics of the lubricants, with the main properties of the specimens detailed in Table 3.1. This investigation followed the guidelines outlined in ASTM G77, which replicate the sliding conditions encountered by engine oils in boundary lubrication systems. The tribological evaluation was conducted in a controlled indoor environment at a temperature of 30°C. Prior to each sliding test, thorough cleaning of both the steel cylindrical block and ring was performed using acetone, followed by drying. The procedures specified in ASTM G77 were implemented utilizing a block and ring tribometer.

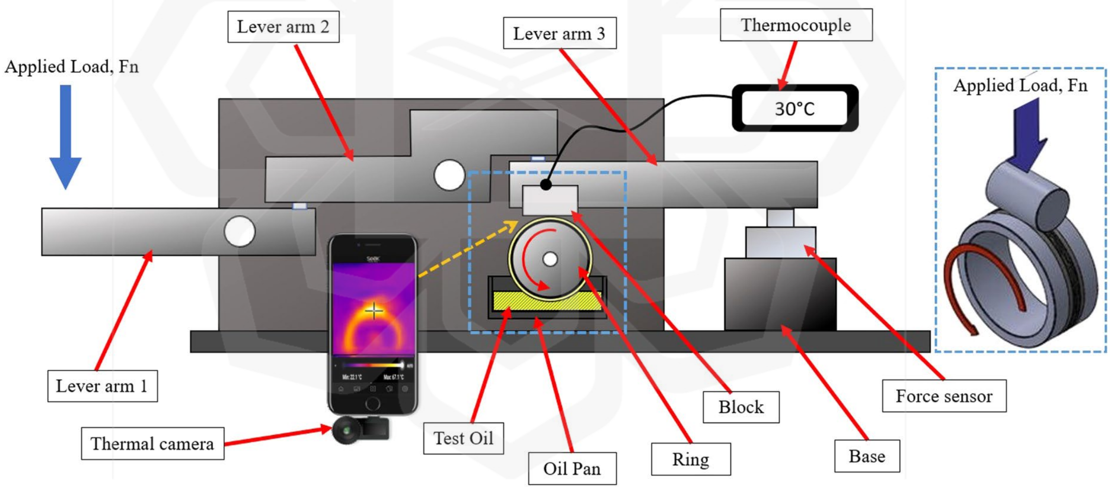

Figure 3.2 ASTM G77 setup to study tribological performance

Table 3.1 General properties of the block and ring

Specimen	Acronym	Material Type and Properties
Block	ø14 × w14 × h14 mm3	AISI 52100 steel • Density ρ=7.81 g/cm3 • Elastic modulus E=210 GPa • Poisson ratio ν=0.3 • Hardness 62 HRC
Ring	ø35 mm× w11 mm	

3.2.2 Lubricants

GO was prepared by dispersing graphene powder into 100 ml of 0W20 lubricant oil using a two-step method, resulting in a dispersion of 0.05wt% graphene. A high sheer homogenizer was employed at 13000 RPM for 45 minutes to achieve a stable dispersion of graphene powder with no agglomeration, as described by Azman et al. (2018). The viscosity of the lubricant was measured at 30°C using an A&D SV-10 vibro-viscometer by A&D Company Ltd, Tokyo, Japan, with an accuracy of 1% and a volume of 30 ml. The same process was repeated for dispersing fullerene powder in 0W20 lubricant oil. Following this, the lubricant oils were assessed for their tribological performance using a Rod and Ring Tribometer under conditions of 490 RPM, 17.7N load, and a sliding distance of up to 900 meters. The comprehensive properties of the commercial lubricants are provided in Table 3.2.

Table 3.2 General properties of the test lubricants

Test Oil	Acronym	Properties
SAE-5W30	5W30	Viscosity @ 40°C=164 mPa.s Density @ 30°C=840 kg/m3
SAE-0W20	0W20	Viscosity @ 40°C=81 mPa.s Density @ 30°C=810 kg/m3
SAE-0W20 + Graphene	GO	-
SAE-0W20 + Fullerene	FO	-

3.3 EXPERIMENTAL PROCEDURES

The ASTM G77 procedures (shown in Figure 3.3) were executed utilizing a block and ring tribometer. Test oils, including 0W20, 5W30, GO and FO, were applied at 60-second intervals over a 45-minute period. To ensure adequate lubrication during the test, the ring is partially immersed in the test oil. This setup allows the oil to be consistently applied to the contact surfaces between the steel block and the ring. A weigh plate of 1.8 kg was positioned on lever arm 1 to maintain a constant load on the block, while a force sensor measured the force on the block via lever arm 2. The steel ring maintained a steady rotational speed of 490 rpm throughout the testing.

To analyze the lubricant's effect on temperature, a SenXorPro© thermal camera monitored the interface temperature as shown in Figure 3.4, while a thermocouple measured the block's temperature during sliding. Mass changes of the steel block were determined after each 60-second interval using an analytical balance. The results for each lubricant type were recorded as shown in Table 3.3. Similar procedures were followed for evaluating the tribological performance of coated steel blocks.

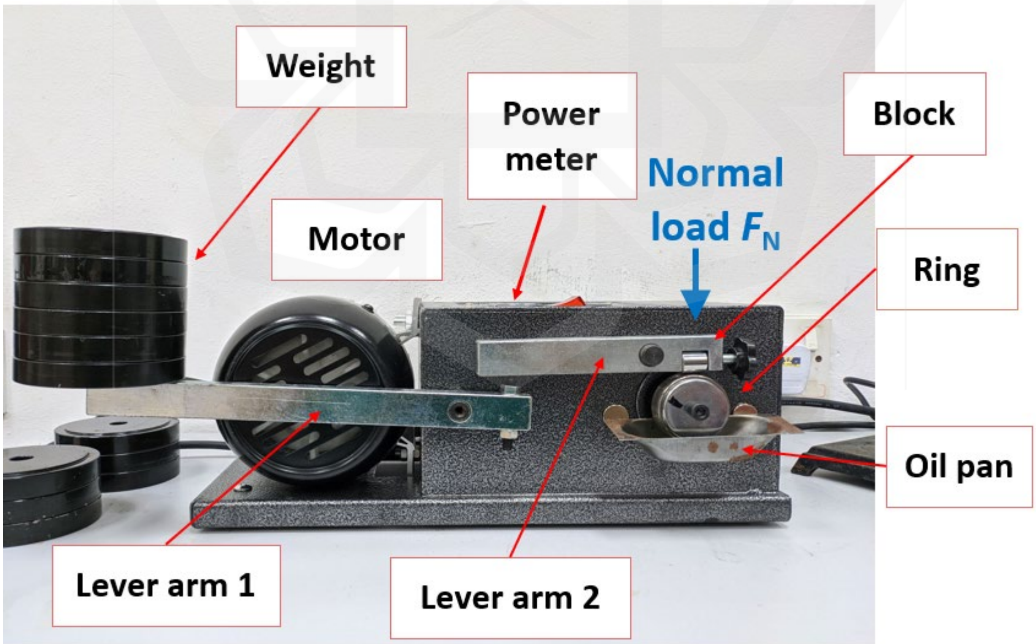

Figure 3.3 ASTM G77 procedure.

Subsequently, the wear severity of the block's friction wear area was assessed using a Dino-Lite digital microscope. Micro-Raman spectroscopy, employing a 488 *nm* wavelength laser for excitation, was utilized to analyze worn surfaces, while Energy-Dispersive X-ray spectroscopy (EDX) was employed to assess elemental composition. Throughout each experiment, friction force was computed, and the friction coefficient was determined using Coulomb's friction law. Additionally, the specific wear rate was calculated with reference to Archard's model.

$$Wear\ Rate,\ K = WH / F_f LN \quad \left(\frac{mm^3}{Nm}\right) \tag{3}$$

Where, W=difference in volume, H=wear rate coefficient, L =sliding distance.

$$Brugger\ Value\ B = F_n / ab \quad \frac{(N)}{mm^2} \tag{4}$$

where F_n =normal force (N), a =length of worn scar area, b =width of worn scar area.

Figure 3.4 Thermal camera set up to monitor interface temperature

Time (s)	0	60	120	180	240	300	360	600	900
Load (Kg) (Constant)	0	1.8	1.8	1.8	1.8	1.8	1.8	1.8	1.8
Temperature									
Block mass (g) - before test									
Block mass (g) - after test									
RPM									
Power (W)									

3.4 DATA PROCESSING

After completion of data collection, the experimental data described in the preceding section were gathered. Following the framework proposed by Hasan et al. (2022), the development of a robust ML model necessitates meticulous data pre-processing. This entails essential techniques such as data normalization, correction of anomalies and missing values, partitioning of data into training and testing sets, and data slicing. The ML algorithm rigorously scrutinized the dataset for irregularities and missing values, making necessary adjustments as required. To mitigate bias or undesirable trends, the data underwent shuffling.

In this study, data cleaning primarily involved eliminating redundant variables, such as constant ones like the material of the block and ring, as well as the applied load. Additionally, certain textual entries like "5W20 oil" or "10W20 oil" posed challenges for Python coding, prompting their conversion into numerical values. Furthermore, since Python simulation processes inputs and outputs sequentially, meticulous preprocessing of each input and output was crucial before advancing to the subsequent stage.

Subsequently, the data underwent partitioning, dividing the entire dataset into a training set and a test set using Python. The training set was utilized for constructing and validating ML models, while the test set assessed model performance with fresh data. The data partitioning followed the recommended method proposed by Hasan et al. (2022), allocating 75% for training and 25% for testing and model validation. During the training phase, the objective was to train the ML model to recognize patterns from the input training dataset and their associated labels. Following this, the test set was utilized to assess and validate the trained classification model.

In this study, three ML, specifically RF, SVR, and DT algorithms. The performance of these models was compared to identify the most effective one. The selection of these three ML models were based on their distinct advantages, particularly in the regression category. DTs are renowned for their interpretability, where each branch represents a decision based on a specific feature. SVR excels in capturing nonlinear relationships and handling complex interactions. RFs are widely acknowledged for their ability to manage complex and high-dimensional data, noisy input features, and nonlinear relationships (Breiman, 2001).

3.5 PARAMETERS OPTIMISATION

An approach aimed at enhancing the performance of ML algorithms involves parameter optimization. In this study, the grid search technique were utilized to identify the optimal parameters. The grid search method, recognized as an optimization tool complementing ML methods, was implemented through a Python script. Grid search is a method for hyperparameter optimization in machine learning. It evaluates all possible combinations of specified hyperparameter values to find the best configuration for model performance (refer Figure 3.4). Each combination is tested, and the one with the optimal metric on the validation set is selected (Ogunsanya et al., 2023). Ranges for several parameters were defined, and the grid search approach systematically tested various combinations of these variables, conducting multiple ML analyses. By assessing model performance across different parameter combinations, the grid search approach suggested the parameters that yielded the most favorable performance.

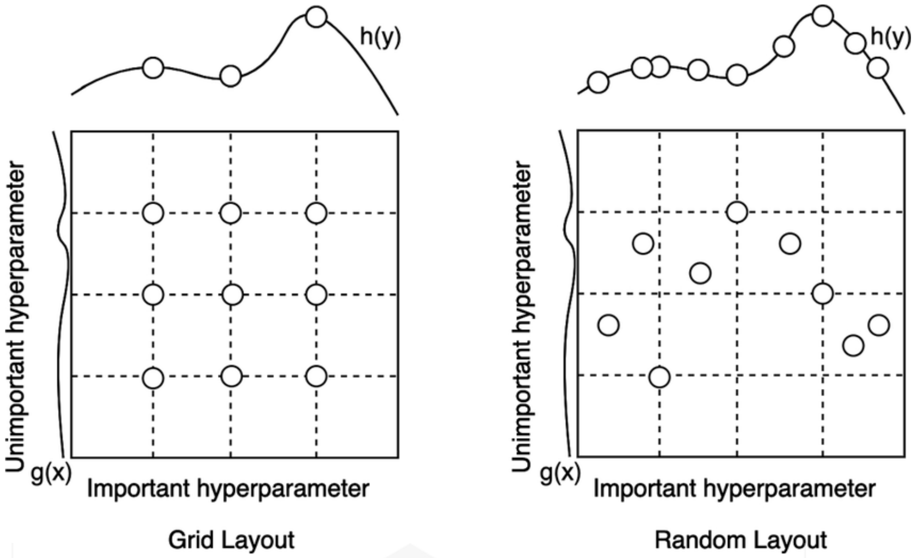

Figure 3.5 Grid Search vs Random Search (Baratchi et al., 2024)

3.6 PERFORMANCE EVALUATION

Performance metrics provide a quantitative evaluation of how well ML models align with real data. In the realm of supervised learning regression problems, the coefficient of determination (R^2) stands out as a crucial performance statistic. R^2 signifies the proportion of data variance that the model can account for, ranging from 0 to 1. An R^2 value of 0 indicates a lack of correlation and the model's inability to explain data variance, while an R^2 of 0.5 suggests a weak correlation, signifying the ML model's limited ability to predict output accurately. Acceptable performance is typically associated with an R^2 value between 0.70 and 0.9, with a value over 0.9 denoting exceptionally acceptable model execution. An R^2 of 1 implies perfect fitting, where the model precisely and error-free describes the variation in the data, though achieving this with experimental data is improbable.

In addition to R^2, other significant measures for evaluating model performance include MAE, MSE, and root mean square error (*RMSE*). *MAE* represents the average difference between expected and actual values. *MSE* is the average of squared discrepancies between actual and projected values of data points, while *RMSE* is the square root of *MSE*. These error values provide crucial insights into model performance, with smaller values indicating greater forecast accuracy for ML models. The formulas for calculating *MAE*, *MSE*, and *RMSE* are as follows:

$$MAE = \frac{1}{N}\sum_{i=1}^{N}|y_i - \hat{y}| \qquad (5)$$

$$MSE = \frac{1}{N}\sum_{i=1}^{N} (y_i - \hat{y})^2 \qquad (6)$$

$$RMSE = MSE = \sqrt{\frac{1}{N}\sum_{i=1}^{N} (y_i - \hat{y})^2} \qquad (7)$$

$$R^2 = 1 - \frac{\sum(y_i - \hat{y})^2}{\sum(y_i - \bar{y})^2} \qquad (8)$$

Where,

y_i - represents the actual values.
$\hat{y}$ - represents the predicted values.
$\bar{y}$ - is the mean of the actual values.
N - is the number of data points.

3.7 SUMMARY

This chapter details the experimental methodology for assessing the tribological performance of selected lubricants and coated bearing steels. It explains the test setup, including the use of ASTM G77 standards for block-on-ring testing, and specifies parameters such as rotational speed, applied load, and sliding distance. Key measurements include the coefficient of friction, wear area, and contact surface temperature. The chapter also describes the preparation and testing of coated bearing steels using materials like TiN, AlTiN, and DLC-AlTiN to investigate their wear resistance and thermal stability. Furthermore, machine learning algorithms—Support SVR, DT and RF—are employed to model and predict friction and wear behavior based on the experimental data. The methodology integrates experimental and computational approaches to provide a robust framework for understanding and optimizing tribological performance.

CHAPTER FOUR

RESULTS AND DISCUSSION

4.1 EFFECTS OF LUBRICANTS ON COF, WORN AREA AND TEMPERATURE

Figure 4.1 – 4.3 show the effects of lubricants and travel distance on COF, temperature and wear area, whereas Figure 4.4 and Figure 4.5 present the analysis of friction coefficient concerning various types of oil in connection with wear scar area, Brugger value, and temperature at a maximum travel distance of 900 m during the test. Figures 4.1 – 4.3 illustrate the influence of lubricant type and travel distance on the coefficient of friction, temperature, and wear scar area.

Figure 4.1 shows the variation of the coefficient of friction for different lubricants as a function of travel distance. Initially, all lubricants exhibit a sharp increase in friction, which stabilizes after about 200 meters. Fullerene oil maintains the lowest coefficient of friction throughout, followed by GO, while conventional lubricants (SAE 0W20 and SAE 5W30) have slightly higher values. This indicates that fullerene oil provides the best lubricity, with GO also offering significant advantages over traditional lubricants in reducing friction over extended travel distances.

Figure 4.2 shows the temperature rise in the lubricated system as travel distance increases. All lubricants show a rapid initial temperature increase, stabilizing beyond 200 meters. However, the conventional oils (SAE 0W20 and SAE 5W30) exhibit significantly higher temperatures, particularly after 600 meters, with SAE 5W30 reaching the highest temperature. GO demonstrates superior thermal performance, with a more stable and lower temperature trend, while fullerene oil also shows better heat resistance than traditional oils, suggesting enhanced heat dissipation properties in these advanced lubricants.

Figure 4.3 highlights the wear characteristics of different lubricants over the travel distance. SAE 0W20 and SAE 5W30 show substantial wear, with the worn scar area increasing significantly, especially beyond 400 meters. In contrast, GO demonstrates exceptional anti-wear performance, with minimal wear throughout the test. Fullerene oil similarly exhibits low wear, but graphene oil outperforms it slightly in terms of maintaining a smaller worn scar area. This suggests that graphene and fullerene oils are more effective in protecting surfaces from wear compared to conventional lubricants, especially under prolonged use.

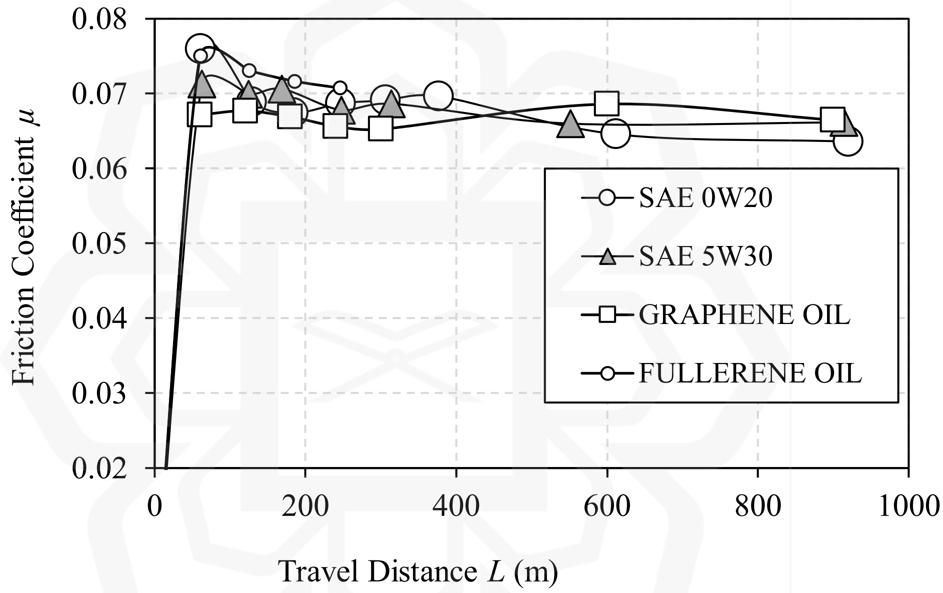

Figure 4.1 Effects of lubricants and travel distance on friction coefficient.

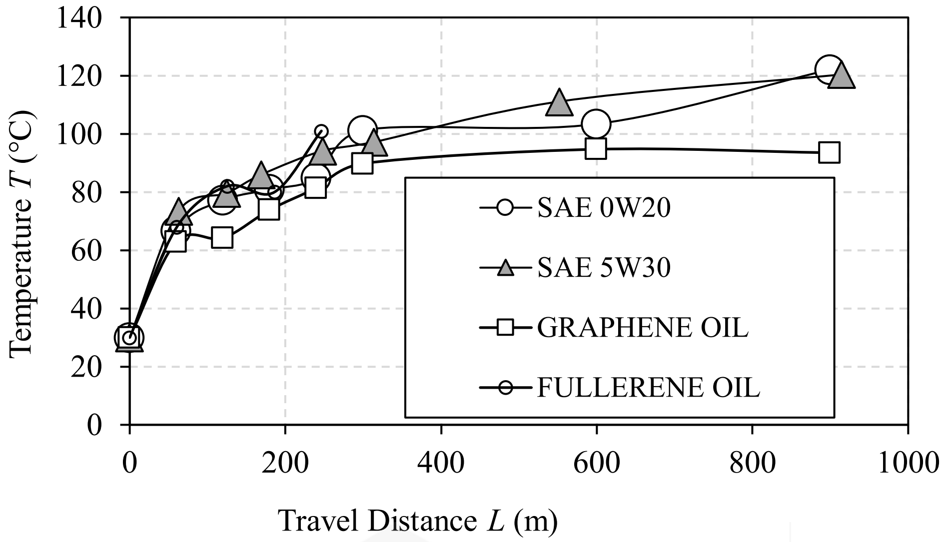

Figure 4.2 Effects of lubricants and travel distance on temperature.

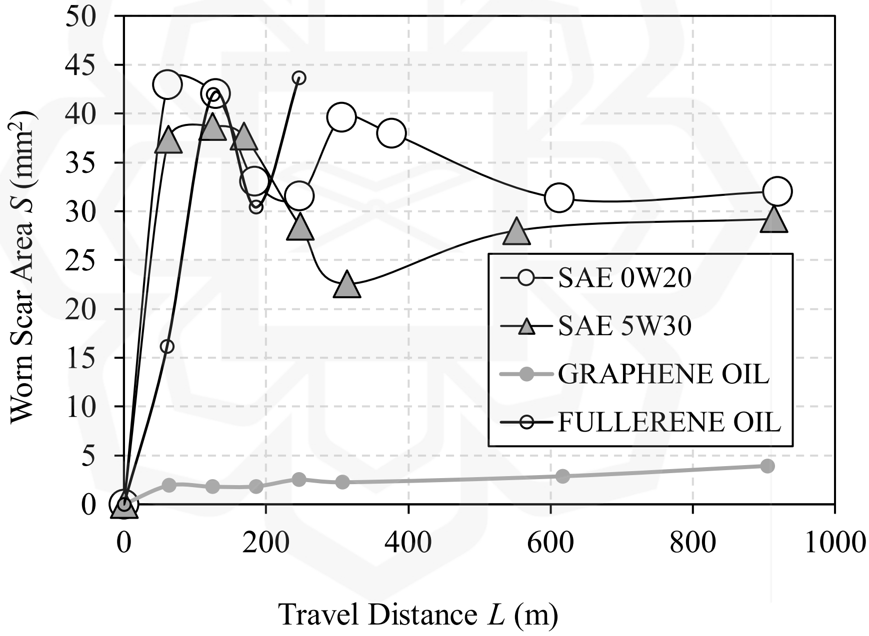

Figure 4.3 Effects of lubricants and travel distance on worn scar area.

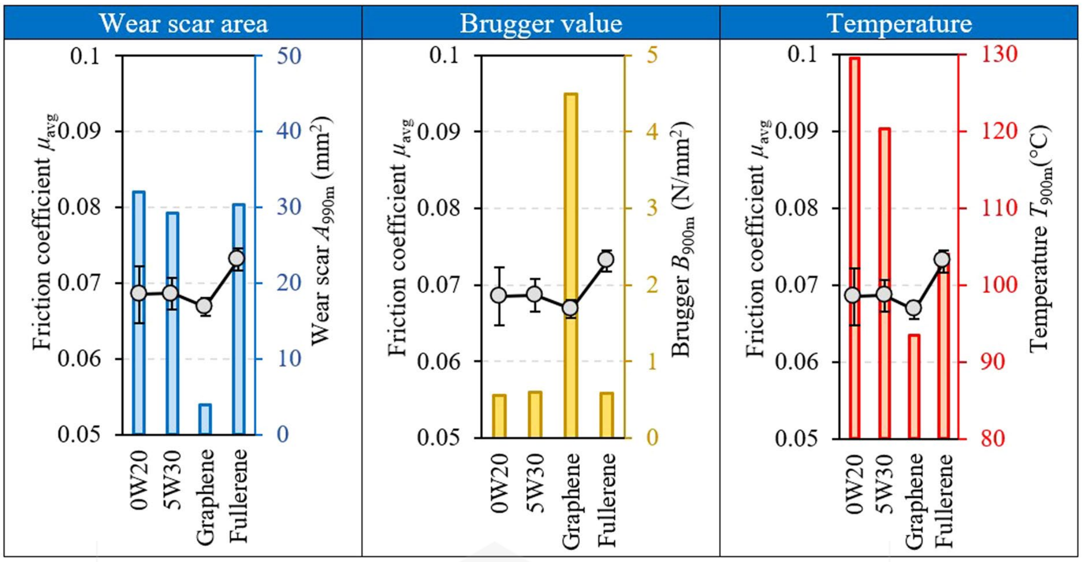

Figure 4.4 The test oils were evaluated at their maximum travel distance of 900 meters where Friction measurements, worn scar area, Brugger value, and temperature were recorded.

The incorporation of graphene into the test oil demonstrates a significant reduction in wear rate compared to other test oils, particularly FO, which exhibited a notable improvement over the baseline 0W20 (see Figure 4.5). It's worth noting that the optimal concentration and size of nanoparticles are closely intertwined with material types and interface properties. Hence, further investigation of FO at various concentrations is recommended to explore its effectiveness as a lubricant additive.

Moreover, the Brugger value for GO was notably higher, indicating the smallest worn scar area, while maintaining a consistent normal load across all test oils. This reduction in friction compared to 0W20 suggests graphene's ability to mitigate interface adhesion and stabilize the surface, consequently reducing the friction coefficient.

Since FO and GO include nanoparticles that increase their heat capacity, their interface temperatures are noticeably lower. FO has a lower interface temperature than 0W20 and 5W30, even though it has the greatest friction coefficient of all the test oils. The effects of graphene and nanoparticle additions in test oils are shown in Figure 4.5, where a notable reduction in wear rate and interface temperature is seen.When graphene or fullerene nanoparticles are added to lubricants, the wear rate is significantly lower than when no additives are used. As studied by Waqas et al., (2021) and Marlinda et al., (2023), the test oil serves as a heat sink, absorbing and dissipating the heat produced by sliding friction. As a result, the temperature at the interface rises with travel distance, reducing wear severity. In particular, GO had the lowest contact temperature among the examined oils, indicating efficient heat dissipation.

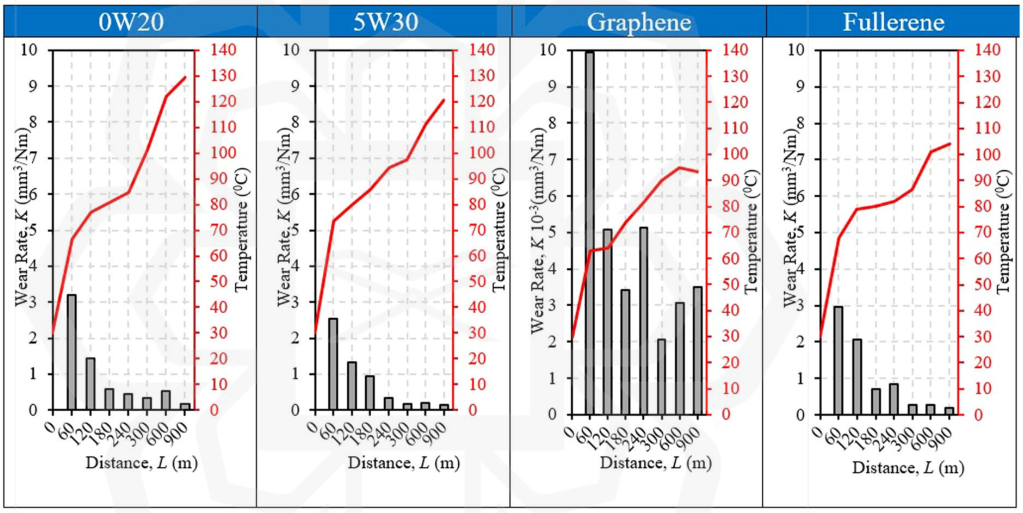

Figure 4.5 The trend of wear rate in relation to increasing travel distances for test oils is influenced by temperature.

Examining wear scar areas through the use of a digital microscope was employed to assess the impact of the nanoparticle additive on lubrication performance. It was observed that the wear scar area on the block treated with GO was notably smaller compared to other test oils, as demonstrated in Figures 4.6 and 4.7. The worn area on the block treated with GO displayed a tidy, shallow, and evenly distributed scar, which can be attributed to the presence of graphene particles in the oil coating the interface contact surface area, thereby preventing direct contact with the ring.

A thin layer of protective lubricant film formed when GO was added to the engine oil as a nanoparticle additive. This resulted in less wear and less direct metal-to-metal contact by enabling smoother shearing of the pressurised graphene-additive oil lubrication film during sliding. The reduced wear scar area observed with GO can be attributed to its ability to form a robust tribofilm on the contact surfaces. Graphene oxide nanoparticles not only provide excellent lubrication but also contribute to the self-healing of the lubricant film during sliding. Their layered structure facilitates smoother shearing, reducing friction and wear significantly. Furthermore, the high thermal conductivity of graphene helps dissipate heat generated during sliding, preventing localized temperature spikes that could degrade the lubricant or damage the surface. This protective mechanism enhances the load-bearing capacity of the lubricant, ensuring consistent performance even under high-stress conditions. These findings demonstrate the effectiveness of GO in extending the lifespan of lubricated components and highlight its potential as an advanced additive in high-performance tribological applications.

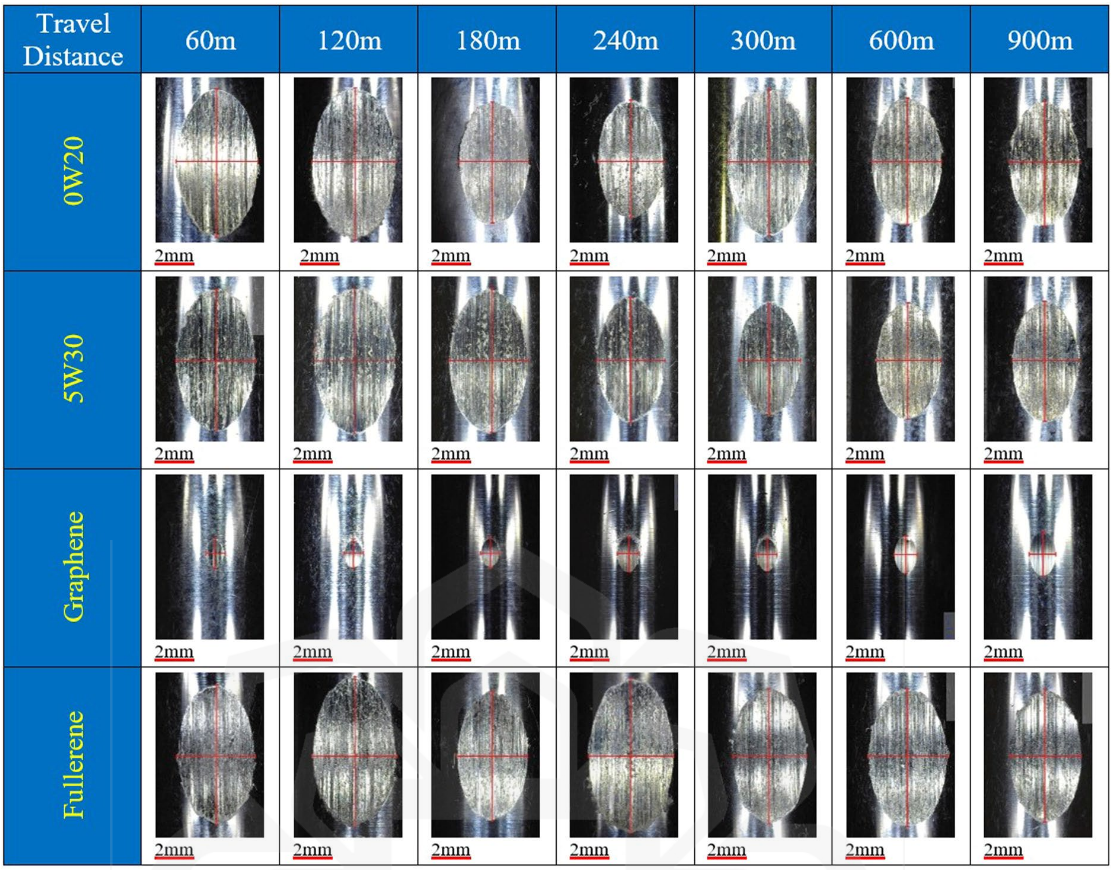

Figure 4.6 Microscopic images of worn area on steel block.

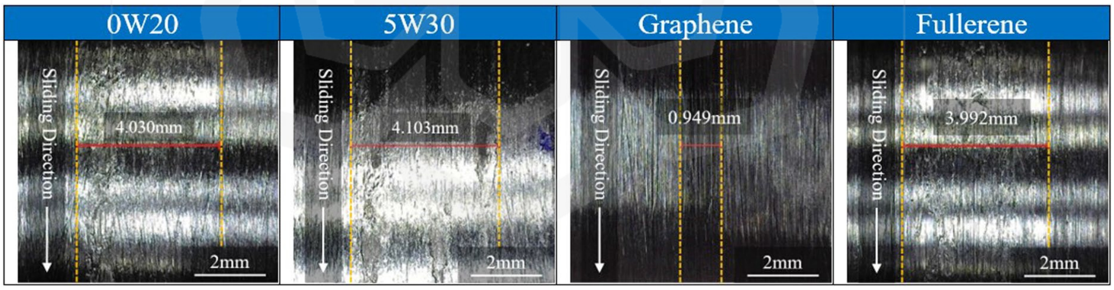

Figure 4.7 Microscopic images illustrating the worn surfaces of the rings for all test oils at a travel distance of 900 meters.

Microscopic assessments performed at a magnification of 50x revealed differences in wear patterns on the steel blocks for each test oil, as shown in Figure 4.8. Between the tribological surfaces, nanoparticles acted as microscopic rollers, enabling the conversion of sliding action into rolling effects and lowering the COF. In contrast to other oils like 0W20, 5W30, and FO, GO showed a notable polishing impact on the steel blocks, resulting in wear tracks with smoother surfaces and less deep grooves.

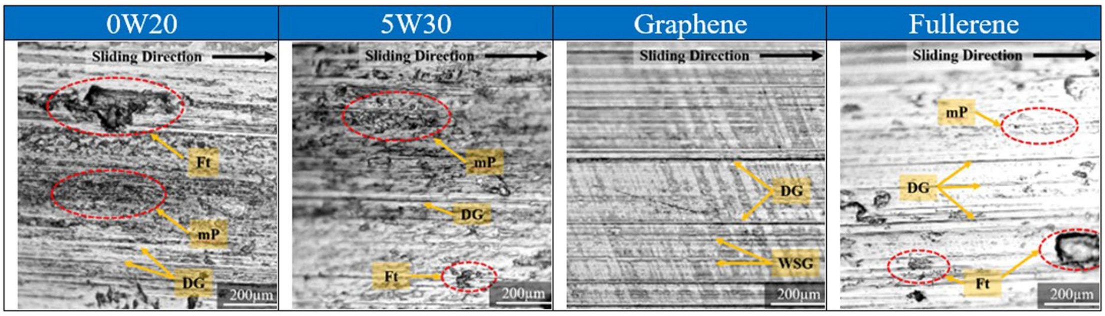

Figure 4.8 Microscopic images of wear area on block surfaces under 50 × magnification. (Notes: DG=deep groove, mP=micro-pits, WSG=wide shallow groove, Ft=fracture).

The purpose of further investigation using Raman spectroscopy was to clarify graphene's function in the wear process. Raman spectroscopy, a technique based on the inelastic scattering of light, is used to study molecular vibrations and material composition, providing a unique fingerprint of substances. Spectral analysis was performed using data from Raman spectroscopy (see Figure 4.9), which were linked to the characteristic graphene peaks (D, G, and 2D). Graphene nanoparticles showed D, G, and 2D bands, confirming their existence on the contact surface, even though debris on the wear track caused a broad fluorescence band and partially obscured several Raman features (see Figure 8). In particular, G band and 2D peaks were observed in GO at 1580 cm−1 and 2300 cm−1, respectively, indicating the existence of graphene nanoparticles.

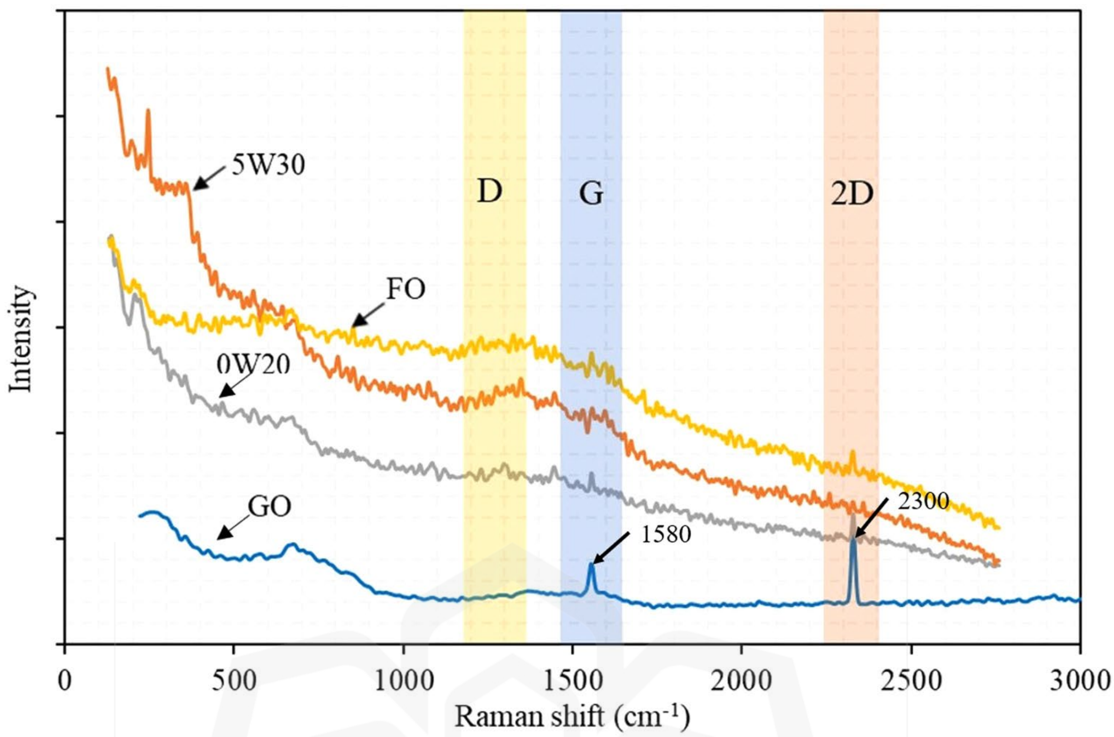

Figure 4.9 Raman spectra for the wear scar area after sliding.

Furthermore, the Energy-Dispersive X-ray (EDX) spectra, which is shown in Figure 4.10, showed clear peaks linked to both graphene and fullerene, suggesting that they are present on the wear scar's surface. An examination of the atomic makeup of the constituents on the wear scar surface indicated a significant carbon content from the lubricant, serving as a wear-prevention barrier. In particular, it was found that the percentages of carbon atoms in graphene and fullerene oils were 52.53% and 75.14%, respectively.

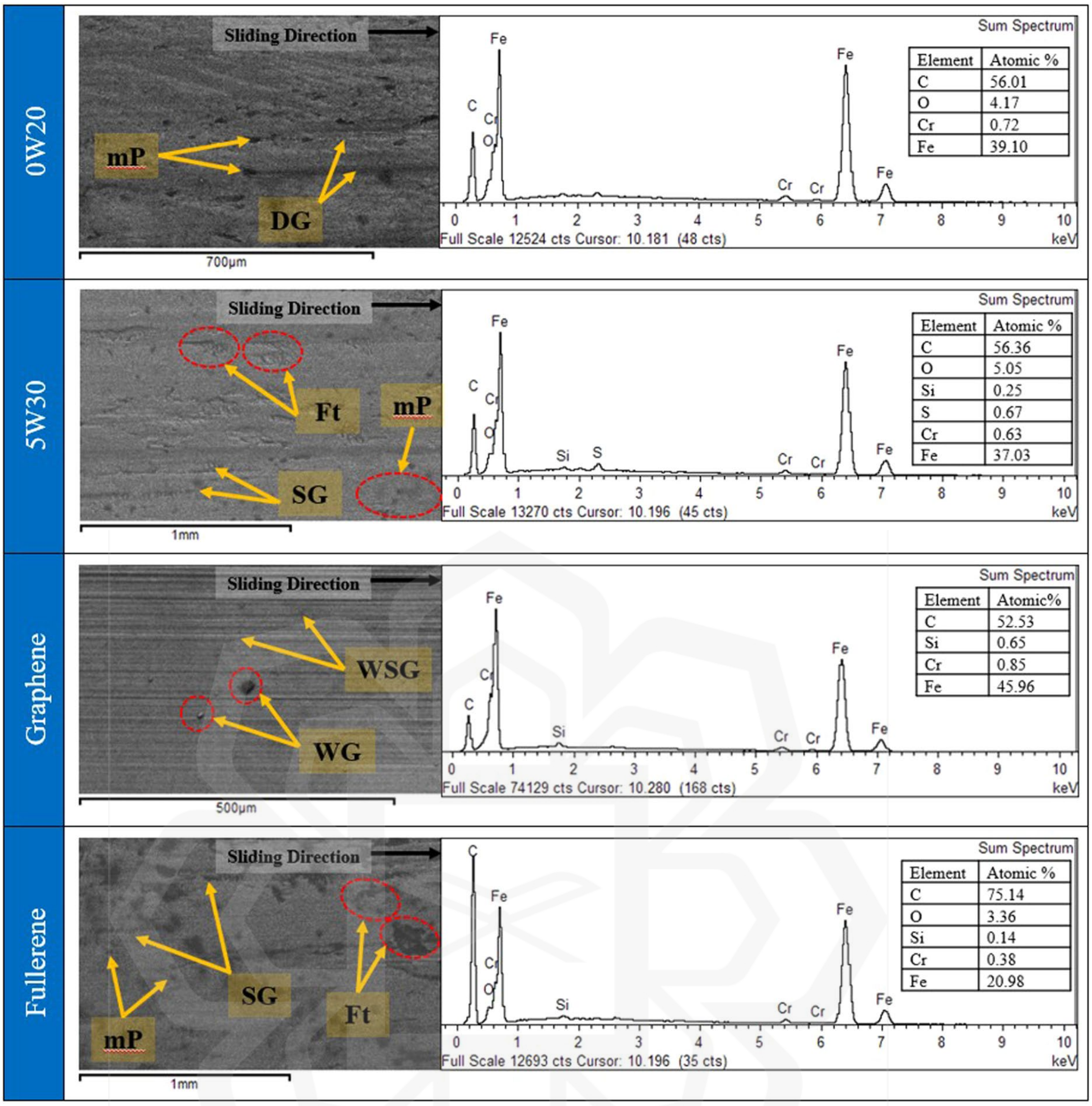

Figure 4.10 SEM images of wear scar area with EDX spectrum and elemental atomic percentage. (Notes: DG=deep groove, mP=micro-pits, SG=shallow groove, WSG=wide shallow groove, WG=welded graphene, Ft=fracture).

4.2 EFFECTS OF COATINGS ON THE STEEL BLOCK ON COF, TEMPERATURE AND WORN AREA

Figures 4.11–4.13 illustrate how various coatings affect temperature, wear area, and coefficient of friction when used as lubricant with GO. As shown in Figure 4.11, the coefficient of friction rises with increasing journey distance. For the majority of coating types, the coefficient of friction remains constant until a travel distance of 3600 metres, increasing to 0.06-0.08 at 60 metres. For all six types of coatings, the coefficient of friction graph generally displayed the same pattern. The similar patterns observed for the coefficient of friction across all coating types can be attributed to their shared fundamental characteristics and operational conditions during the test. All the coatings, such as TiN, AlTiN, CrN, TiAlSN, TiCN, and DLC-AlTiN, are engineered to reduce friction and wear through mechanisms like surface hardness, smoothness, and chemical stability. These coatings form a protective layer that minimizes direct metal-to-metal contact, resulting in comparable frictional behavior during the initial phases of sliding.

The consistent rise in the coefficient of friction after a travel distance of 3600 meters could be due to wear or degradation of the coatings under prolonged contact stress and sliding conditions. This suggests that while the coatings initially perform uniformly, their wear resistance and the ability to maintain a lubricated interface become critical over extended distances. Additionally, factors like test parameters (load, speed, and lubrication) and the inherent properties of the coatings, such as adhesion and thermal stability, contribute to the observed similarities in frictional patterns. These patterns indicate that the coatings are optimized for similar tribological performance under the specified testing conditions.

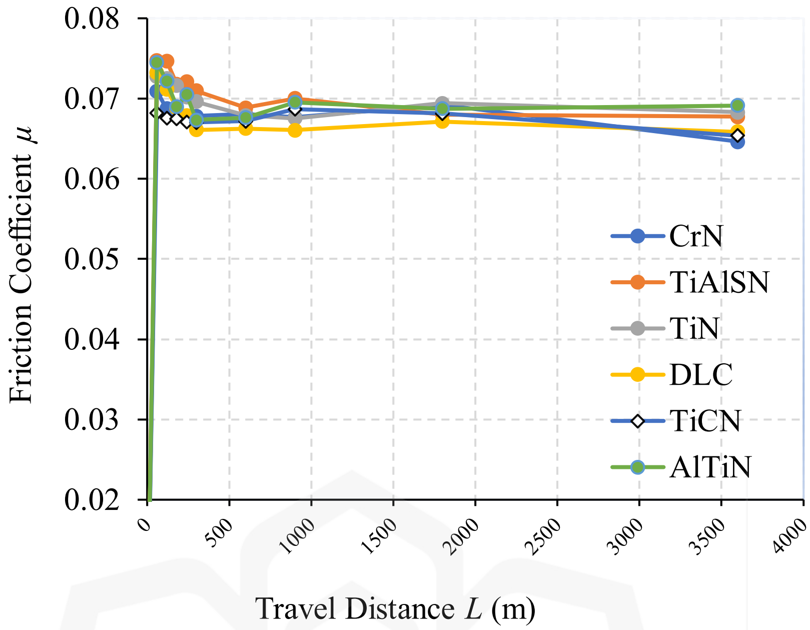

Figure 4.11 Effect of coatings and travel distance on friction coefficient.

Figure 4.12 shows the trend of lubricant temperature against travel distance for six different coated steel block under GO as lubricant. From this figure, when travel distance increases, the lubricant temperature also increases. The lubricant temperature increases from 30 degree Celsius to 123-157 degree Celsius. DLC coated block steel showed the highest temperature, whereas CrN coated steel showed the lowest temperature. In general, the temperature graph for the lubricant exhibited a consistent upward trajectory across all six coatings. This can be attributed to the gradual accumulation of heat generated by friction between the sliding couples, leading to a progressive rise in the lubricant temperature over time. The increase in lubricant temperature with travel distance is caused by frictional heat generated at the sliding interface. DLC-coated steel blocks showed the highest temperature due to lower thermal conductivity, which retains more heat. In contrast, CrN-coated blocks, with better heat dissipation properties, resulted in the lowest temperatures. The consistent rise in temperature for all coatings reflects the accumulation of heat over time, emphasizing the role of coating material properties in managing frictional heating during extended operation.

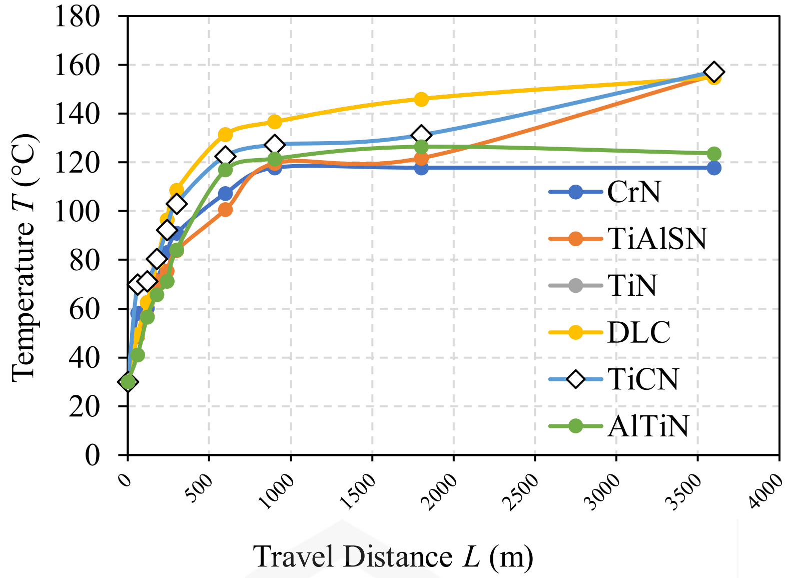

Figure 4.12 Effects of coating and travel distance on temperature.

The wear volume loss represents the variation in volume and weight resulting from sliding wear during the block on ring test. As depicted in Figure 4.13 and Table 4.1, differences in worn area loss were observed among the six differently coated steel blocks. Notably, the CrN-coated block exhibited the highest worn area loss compared to the other coatings, while the AlTiN-coated block demonstrated the lowest wear volume loss. This suggests that the CrN-coated block experienced more rapid wear, leading to increased wear volume loss. The higher wear volume loss in the CrN-coated block indicates its reduced resistance to prolonged sliding, likely due to surface roughness or brittleness. In contrast, the AlTiN-coated block's minimal wear loss highlights its superior hardness and stability under high load and temperature, making it more effective at reducing material removal during sliding wear. These differences reflect the varying suitability of coatings under specific operating conditions.

Table 4.1 Comparison of worn area of steel block using different coatings.

Time	60s	120s	180s	240s	300s	600s	900s	1800s	3600s
CrN (mm^2)	7.5964	18.4453	10.5421	18.6052	9.3248	9.3762	15.1869	37.2445	110.141
TiAlSN (mm^2)	2.3368	1.1928	1.8439	1.8341	3.6079	4.0637	4.7815	5.44332	18.6658
TiN (mm^2)	2.7920	2.8069	3.0851	3.4305	3.4304	7.1236	9.8948	11.9918	32.6078
DLC (mm^2)	2.6063	2.69378	2.4814	1.4644	2.1954	3.0146	7.1425	6.54969	22.9208
TiCN (mm^2)	2.5250	2.6526	2.7548	2.8538	2.9579	3.4402	3.4214	5.54186	17.8448
AlTiN (mm^2)	1.8791	1.7259	1.2997	1.9031	2.1118	2.1118	2.6959	4.97812	5.5357

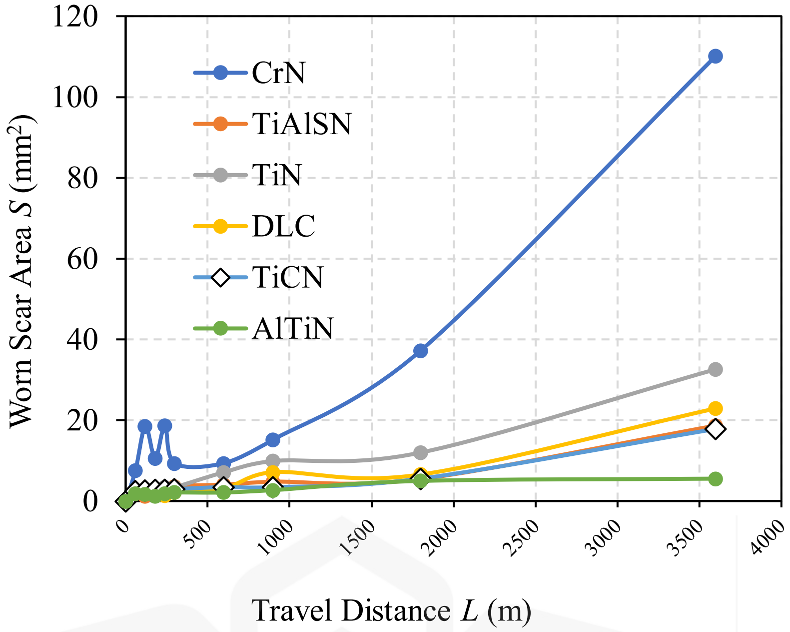

Figure 4.13 Effects of coatings and travel distance on worn scar area

4.3 PERFORMANCE OF ML MODELS FOR COF

Table 4.1 summarizes ML model performance in predicting the COF. R^2 scores for test sets range from 0.7828 to an unexpected -84.2046. R^2 measures how well models capture variance, with higher values indicating better performance. Notable R^2 variation suggests differing success in capturing COF patterns.

The RF model achieved the highest R^2 value of 0.7828 for predicting the COF, indicating good performance. This model exhibits 78% accuracy in predicting COF for steel blocks and tribological test factors. The MSE, MAE, and RMSE values for this model were impressively low at 9.4970, 0.0022, and 0.0031, respectively, indicating high prediction accuracy.

The DT model also performed well, with nearly identical metrics to RF, except for a slightly different MSE. Both models showcase satisfactory predictive capabilities.

However, the SVR model exhibited notable deviations in MSE, MAE, RMSE, and an unexpected negative R^2 value of -84.2046. This negative R^2 value may stem from inaccuracies in experimental results and datasets, suggesting potential issues with the SVR model's performance under certain conditions.

Figure 4.14 – 4.16 show comparison of actual and prediction of COF over observation number for RF, SVR and DT models respectively. Figure 4.14 shows a comparison between the actual and predicted COF using the RF model. The predicted COF values align closely with the actual ones, confirming that the model is effective in capturing the frictional behavior under the tested conditions. A few discrepancies are visible, particularly where the predicted values deviate at higher observation numbers, suggesting occasional overestimation or underestimation. Despite these minor differences, the overall prediction accuracy indicates that RF is a suitable algorithm for forecasting COF in tribological experiments. The two figures compare the performance of the SVR model and the DT model in predicting the COF.

Figure 4.15, corresponding to the SVR model, shows a considerable mismatch between the actual (blue dots) and predicted (red dots) values, with high fluctuations in the predicted values across observations. This indicates that the SVR model fails to capture the underlying pattern accurately, leading to poor prediction consistency. In contrast, in Figure 4.16, which represents the DT model, demonstrates a much closer alignment between the actual and predicted values. The predicted values (red dots) follow the actual trend (blue dots) with reduced deviations, suggesting that the DT model provides a more accurate and stable prediction of the COF compared to the SVR model. In summary, RF and DT models demonstrate strong predictive accuracy for COF, while SVR's unexpected results warrant further investigation into experimental accuracy and dataset reliability.

Table 4.2 Comparison of ML models for COF

ML model	Mean Squared Error (*MSE*)	Mean Absolute Error (*MAE*)	Root Mean Squared Error (*RMSE*)	R- Squared Value (R^2)
Random Forest	9.4970	0.0022	0.0031	0.7828
Support Vector Regression	0.0037	0.0560	0.0610	-84.2046
Decision Tree	1.3517	0.0023	0.0037	0.6909

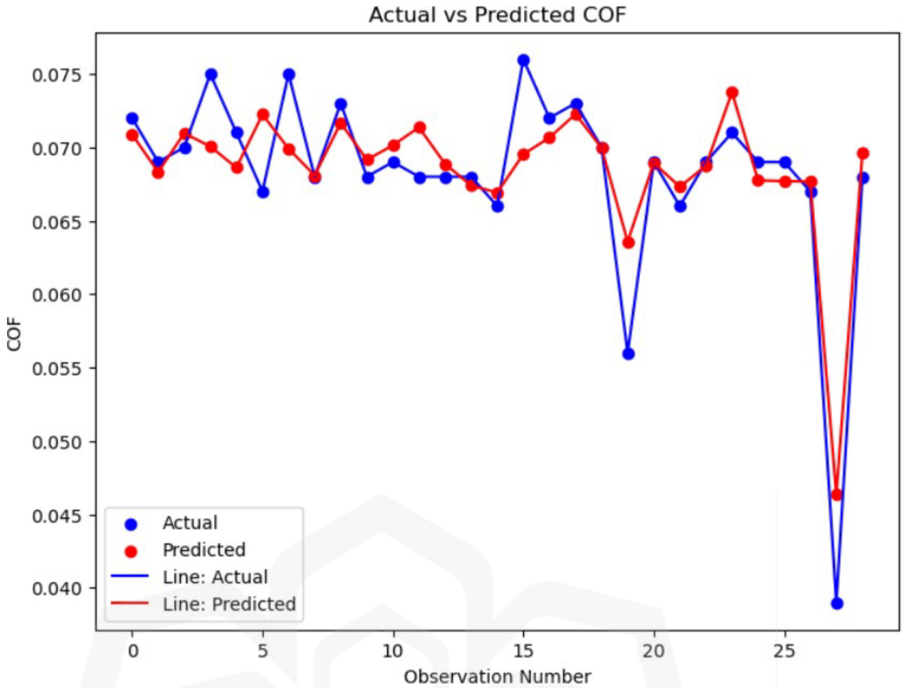

Figure 4.14 Actual vs. Predicted Value of COF by RF Model.

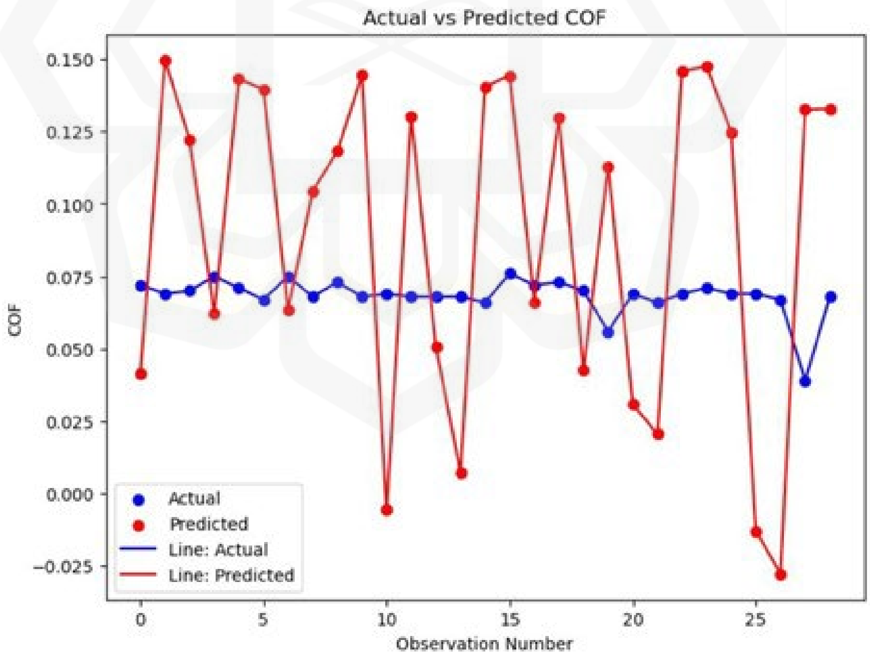

Figure 4.15 Actual vs. Predicted Value of COF by SVR Model.

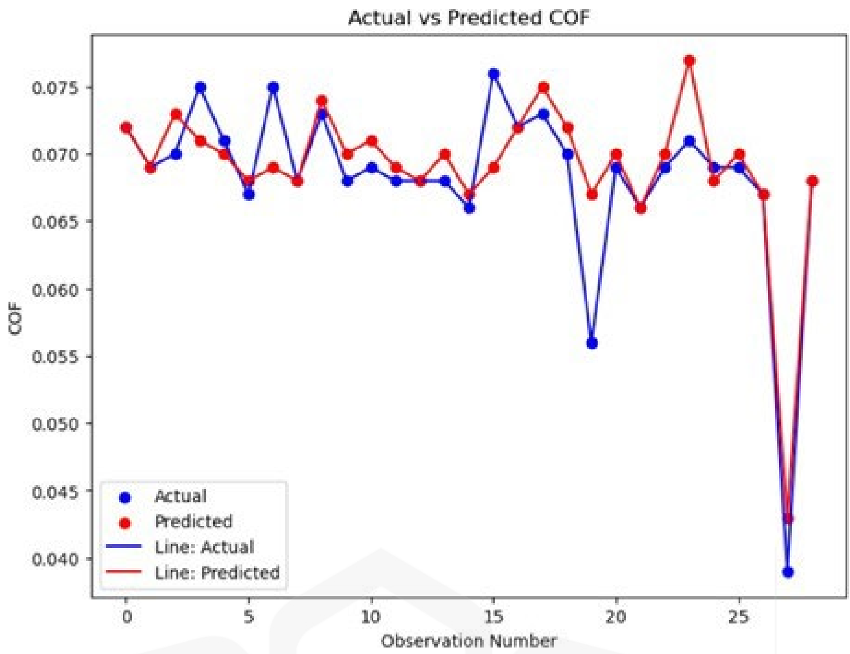

Figure 4.16 Actual vs. Predicted Value of COF by DT model.

4.4 PERFORMANCE OF ML MODELS FOR WORN AREA

Table 4.2 shows ML model performance in predicting the Worn Area. The R^2 values on test sets ranged from 0.2797 to 0.8270 for the ML models. The MSE ranged between 54.0492 and 224.9788, MAE ranged between 4.2374 and 9.5836, and RMSE varied between 7.3518 and 14.9993. Among the models, RF recorded the highest R^2 value, which is 0.8270. This indicates that the RF model successfully identified the worn area of the block. Meanwhile Figure 4.17 – 4.19 show the comparison of prediction and actual worn area of the steel block for RF, SVR and DT models respectively.

Figure 4.17, the actual versus predicted wear area values for the RF model show a good fit, indicating that RF can predict wear characteristics accurately. Similarly, the DT model (Figure 4.19) also provides a reliable prediction with minimal deviation from actual values. However, the SVR model, as shown in Figure 4.18, struggles significantly, with a poor alignment between predicted and actual wear areas. The R^2 value of 0.2797 further supports this, suggesting a weak model fit. The reason for SVR's lower performance could be its limitations in handling non-linear relationships in the data, compared to RF and DT, which better capture the complexity of the wear patterns. The fluctuating predictions from SVR indicate it cannot generalize well for this dataset.

Table 4.3 Comparison of ML models for Worn Area

ML model	Mean Squared Error (*MSE*)	Mean Absolute Error (*MAE*)	Root Mean Squared Error (*RMSE*)	R- Squared Value (R^2)
Random Forest	54.0492	4.7657	7.3518	0.8270
Support Vector Regression	224.9788	9.5836	14.9993	0.2797
Decision Tree	63.5641	4.2374	7.9727	0.7965

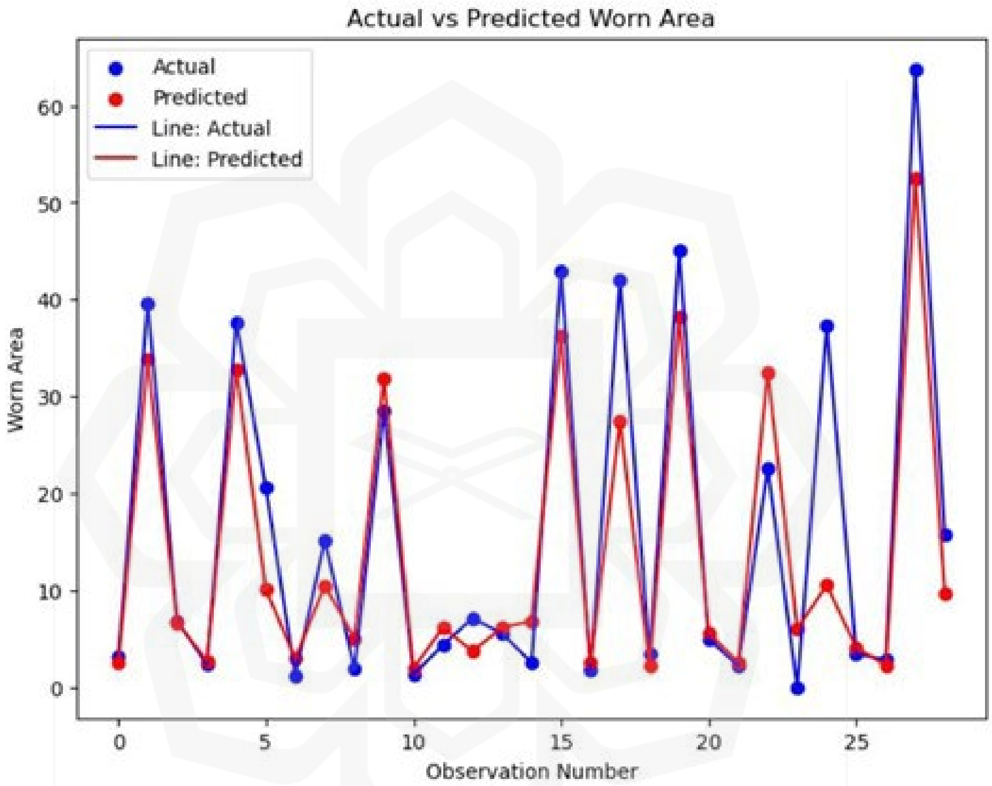

Figure 4.17 Actual vs. Predicted Value of Worn Area by RF Model.

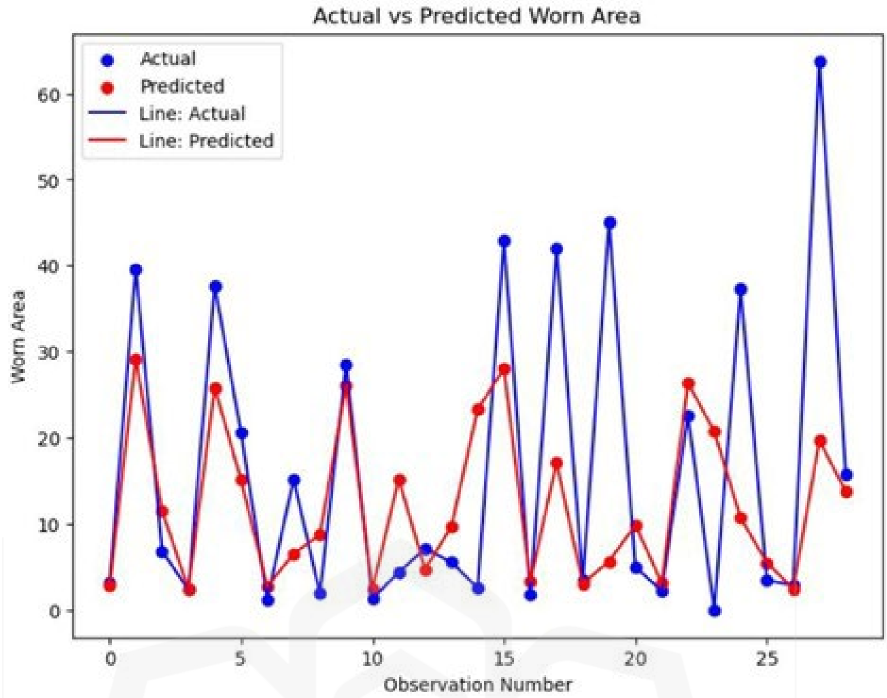

Figure 4.18 Actual vs. Predicted Value of Worn Area by SVR Model.

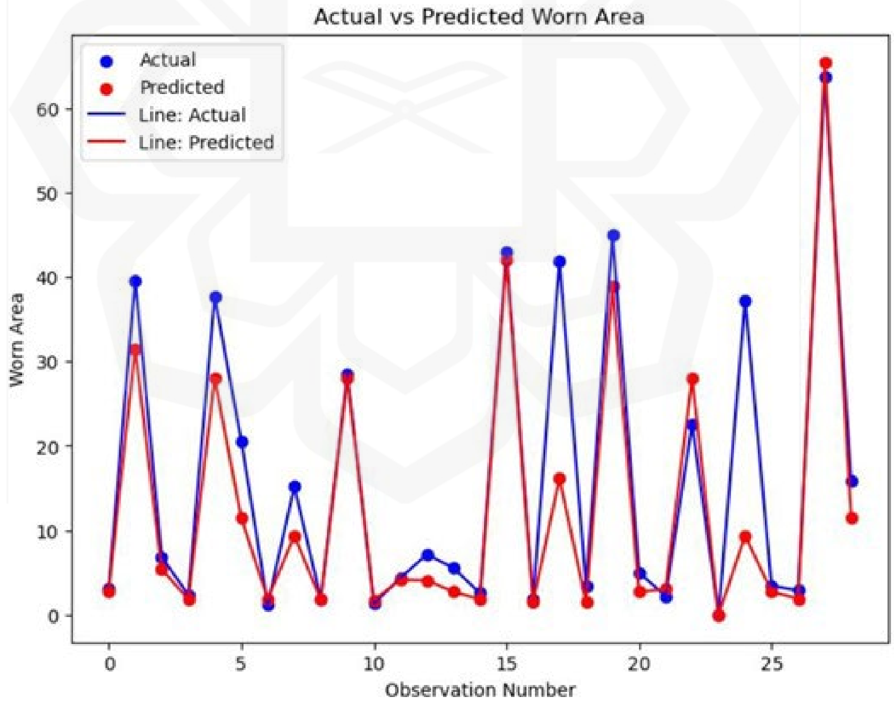

Figure 4.19 Actual vs. Predicted Value of Worn Area by DT model.

4.5 PERFORMANCE OF ML MODELS ON STEEL BLOCK TEMPERATURE

The performance indicators for ML models used to predict steel block temperatures are presented in Table 4.3. The test sets for the ML models exhibit R^2 values ranging from 0.1935 to 0.8250. In terms of MSE, MAE, and RMSE, the ranges were 212.1415 to 977.6777, 9.0818 to 21.4694, and 14.5651 to 31.2678, respectively. Notably, the DT model achieved the highest R^2 value of 0.8250, signifying an 83% accuracy rate in predicting the temperature of a steel block.

On the other hand, the SVM model recorded the lowest R^2 value of 0.1935, indicating a lower correlation and suggesting that the ML model may be less effective in forecasting the output temperature. Figure 4.20 compares the actual and predicted temperatures using the RF model, showing a strong alignment between the two, indicating that RF effectively predicts temperature variations in the tribological system. The DT (Figure 4.22) also exhibits good predictive accuracy, with predicted temperatures closely matching actual measurements. However, Figure 4.21, representing the SVR model, reveals a significant discrepancy between the predicted and actual values, with larger fluctuations observed. This poor performance could be due to SVR's sensitivity to the choice of kernel function and hyperparameters, which may not be optimally tuned for this specific dataset. Additionally, SVR may struggle with capturing complex non-linear relationships as effectively as RF or DT in this context. Despite these differences, both RF and DT models demonstrate stronger suitability for temperature prediction in tribological experiments compared to SVR.

Table 4.4 Comparison of ML models for Lubricants Temperature

ML model	Mean Squared Error (*MSE*)	Mean Absolute Error (*MAE*)	Root Mean Squared Error (*RMSE*)	R- Squared Value (R^2)
Random Forest	338.0329	10.1399	18.3857	0.7212
Support Vector Regression	977.6777	21.4694	31.2678	0.1935
Decision Tree	212.1415	9.0818	14.5651	0.8250

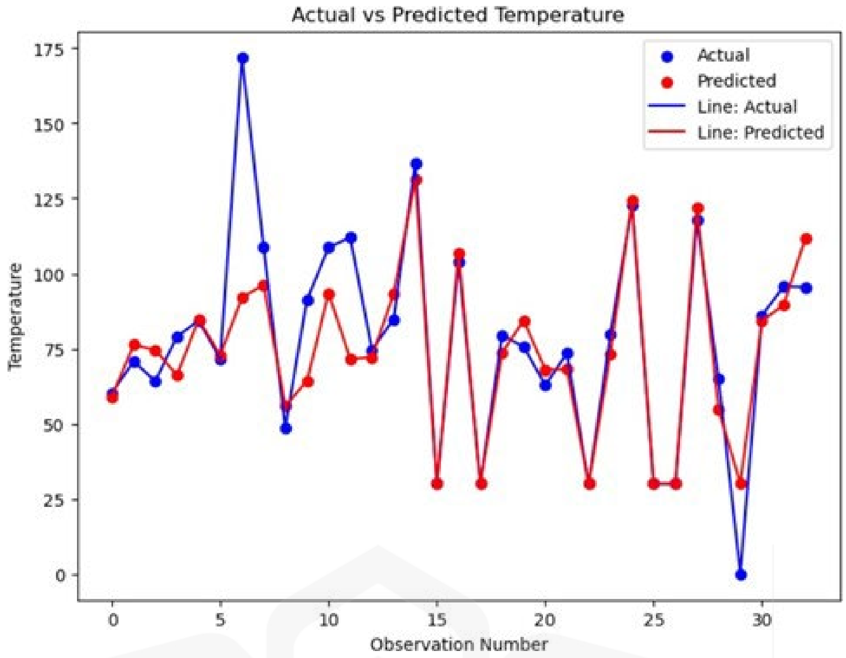

Figure 4.20 Actual vs. Predicted Value of Lubricant Temperature by RF Model.

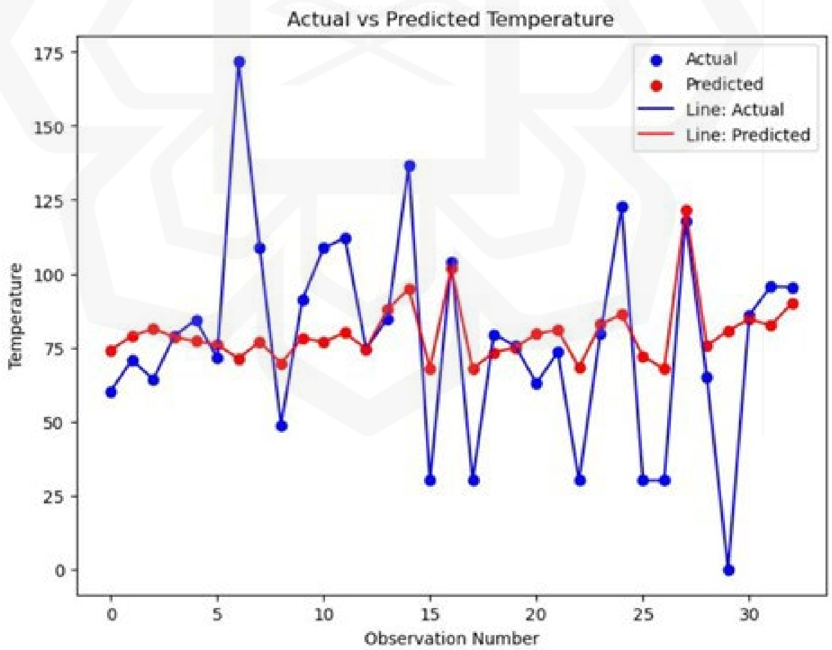

Figure 4.21 Actual vs. Predicted Value of Lubricant Temperature by SVR Model.

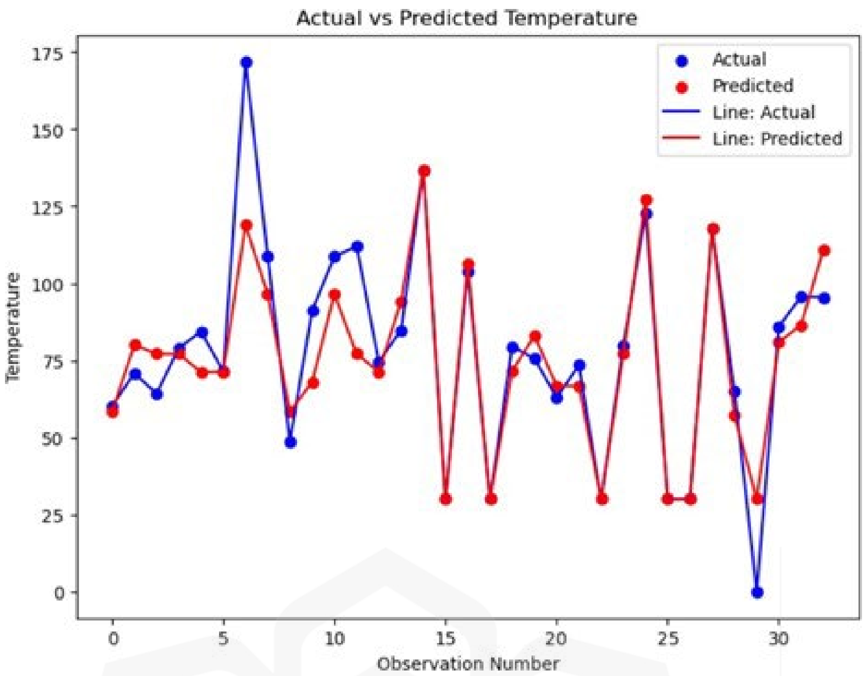

Figure 4.22 Actual vs. Predicted Value of Lubricant Temperature by DT model.

4.6 DISCUSSION

The present study aims to investigate the effects of various lubricants on key parameters related to metal-to-metal interactions, namely the coefficient of friction, temperature, and wear area. Through the utilization of a block on ring test, this study focuses to elucidate the impacts of different lubricants on these critical factors. Specifically, the lubricants are 5W10 oil, 10W20 oil, and graphene and fullerene oil. The findings of this investigation highlight graphene as the most effective lubricant for non-coated steel blocks. Its application demonstrates superior performance in reducing the coefficient of friction, managing temperature, and minimizing wear area compared to other lubricants examined.

Furthermore, this study investigates into exploring the effects of coating on steel blocks when employing graphene as a lubricant. The coated steel blocks, including TiN, AlTiN, CrN, TiAlSN, TiCN, and DLC-AlTiN, are subject to thorough analysis. In terms of the coefficient of friction, the study reveals a consistent trend with slight variations as the travel distance increases across different coatings. Interestingly, the use of graphene as a lubricant yields comparable outcomes among the coated steel blocks. Regarding temperature effects, CrN emerges as the coating material demonstrating the lowest temperature, while DLC-AlTiN exhibits the highest temperature. This elucidates the differential thermal management capabilities of various coatings in conjunction with graphene lubrication.

Moreover, the investigation shows significant differences in wear area among the coated steel blocks. Notably, CrN exhibits the highest wear area, highlighting the role of coating materials in influencing wear characteristics in metal-to-metal applications. Previous studies have demonstrated that graphene enhances lubricant performance by reducing friction and wear, as it forms a protective film that minimizes metal-to-metal contact (Marlinda et al., 2023). In this study, graphene exhibited superior performance, aligning with findings from similar tribological tests. Coatings like TiN and DLC are known for improving wear resistance and friction reduction. In line with past research, CrN coatings showed higher wear volumes, likely due to lower hardness or weaker adhesion (Ibrahim et al., 2024). Overall, these results confirm graphene's effectiveness and highlight the critical role of coating selection in tribological applications. In summary, this study provides comprehensive insights into the effects of lubricants and coatings on critical parameters such as friction coefficient, temperature, and wear area.

The performance evaluation of machine learning models in predicting critical parameters such as coefficient of friction, temperature, and worn area is critical in this study. Utilizing data from the earlier sections, three machine learning models are assessed: SVR, RF and DT. In terms of predicting the coefficient of friction, RF exhibits the most promising performance, as indicated by the highest R^2 value of 0.7828. The R^2 value, ranging from 0 to 1, serves as a measure of the model's capability in making predictions. A higher R^2 value suggests a better fit of the model to the data, implying RF's proficiency in capturing the underlying patterns associated with coefficient of friction.

Next, the prediction of worn area, RF once again emerges as the top-performing model, having an R^2 value of 0.8270. This high R^2 value underscores RF's effectiveness in accurately predicting worn area based on the given data. Such precision in prediction holds significant implications for understanding wear characteristics and facilitating proactive maintenance strategies in metal-to-metal applications.

Meanwhile, when assessing the effects of temperature, DT showed the highest R^2 value of 0.8250. This indicates DT's robust performance in capturing the nuanced relationships between various factors influencing temperature variations. The model's capability in elucidating temperature dynamics is crucial for optimizing thermal management strategies in metal-to-metal interactions. These findings underscore the significance of employing appropriate machine learning techniques tailored to specific parameters, thus enhancing the predictive accuracy and informing decision-making processes in industrial applications.

4.7 SUMMARY

This chapter explores the influence of lubricants and coatings on friction, temperature, and wear in tribological systems. It demonstrates how GO improves performance by lowering the coefficient of friction, reducing wear area, and managing temperature more effectively than other lubricants. Additionally, the effects of coatings like TiN, CrN, and DLC-AlTiN on wear and temperature are analyzed, showing notable differences in wear volume and thermal behavior across different materials. The chapter also highlights the predictive power of machine learning models, particularly RF, in forecasting these tribological parameters. These findings emphasize the importance of selecting optimal lubricants and coatings for better performance in industrial applications, with machine learning offering valuable insights for optimization.

CHAPTER FIVE

CONCLUSION AND RECOMMENDATIONS

5.1 CONCLUSION

In conclusion, this study successfully achieved its three primary objectives:

Firstly, the investigation into the effects of lubricants on the coefficient of friction, worn area, and temperature generated a comprehensive dataset, revealing that the addition of graphene to 0W20 oil resulted in significant improvements. GO reduced friction and wear, while also demonstrating superior heat dissipation, as reflected by the lowest interface temperature compared to the other lubricants.

Second, the study developed a dataset to examine the effects of various coatings on the same tribological parameters. While all coatings showed similar trends in friction behavior, CrN coatings stood out, exhibiting lower temperatures but higher wear area. This highlighted the role of coatings in affecting not only wear but also thermal management during sliding interactions.

Finally, machine learning models were employed to predict and validate the coefficient of friction, worn area, and temperature. The RF model performed best for predicting both the coefficient of friction and wear area, while the DT model excelled at predicting temperature. These findings demonstrate the potential of machine learning in enhancing the predictive accuracy of tribological behavior based on lubricant and coating properties.

Overall, this study contributes to optimizing lubrication strategies and improving predictive capabilities in tribology, offering a clearer path toward enhancing engine durability and performance through data-driven approaches.

5.2 RECOMMENDATIONS

Future studies should look into the influence of different substrate materials on tribological performance. By testing various substrates, we can gain a better understanding of how coatings and lubricants perform across different materials, which could lead to new insights and improve machine learning models for predicting tribological behavior.

Another area for further research would be to use reciprocating-type tribometers. These devices can better simulate real-world conditions, providing more detailed data that could improve the accuracy of machine learning predictions by introducing a wider range of testing scenarios.

Additionally, future research should explore how machine learning models perform across different lubrication modes, such as boundary, mixed, and hydrodynamic lubrication. This would help refine the models, making them more consistent and reliable for various industrial applications.

REFERENCES

Albatayneh, A., Assaf, M. N., Alterman, D., & Jaradat, M. (2020). Comparison of the overall energy efficiency for internal combustion engine vehicles and electric vehicles. Rigas Tehniskas Universitates Zinatniskie Raksti, 24(1), 669-680

Almen, J. O. (1950), in Mechanical Wear (ed. J. T. Burwell) American Society of Metals, pp. 229–288.

Alloghani, M., Al-Jumeily, D., Mustafina, J., Hussain, A., & Aljaaf, A. J. (2020). A Systematic Review on Supervised and Unsupervised Machine Learning Algorithms for Data Science. In M. W. Berry, A. Mohamed, & B. W. Yap (Eds.), Supervised and Unsupervised Learning for Data Science (pp. 3–21). Springer International Publishing.

Aydin, F., & Durgut, R. (2021). Estimation of wear performance of AZ91 alloy under dry sliding conditions using machine learning methods. Transactions of Nonferrous Metals Society of China, 31(1), 125–137.

Azman, N. F., Syahrullail, S., & Rahim, E. A. (2018). Preparation and dispersion stability of graphite nanoparticles in palm oil. Jurnal Tribologi, 19, 132–141.

Baratchi, M., Wang, C., Limmer, S., van Rijn, J., Hoos, H., Bäck, T., & Olhofer, M. (2024). Automated machine learning: past, present and future. *Artificial Intelligence Review*, *57*. https://doi.org/10.1007/s10462-024-10726-1

Bhushan, B. (2013). Introduction to Tribology (2nd ed.). New York: Wiley.

Das, S., Dey, A., Pal, A., & Roy, N. (2015). Applications of artificial intelligence in machine learning: review and prospect. International Journal of Computer Applications, 115(9).

Gee, chuen-ming & Tseng, Chienchih & Wu, F-Y & Lin, C-T & Chang, Hsin-Ping & Li, L-J & Chen, J-C & Hu, Lung-Hao. (2014). Few layer graphene paper from electrochemical process for heat conduction. Materials Reseach Innovations. 18. 208.

Ghalme, S., Koinkar, P., & Bhalerao, Y. (2020). Tribology in Industry Effect of Aluminium Oxide (Al2O3) Nanoparticles Addition into Lubricating Oil on Tribological Performance. Tribology in Industry, 42, 494–502.

Hasan, M. S., Kordijazi, A., Rohatgi, P. K., & Nosonovsky, M. (2022). Machine learning models of the transition from solid to liquid lubricated friction and wear in aluminum-graphite composites. Tribology International, 165, 107326.

Hasan, S., Hasan, M. S., Kordijazi, A., Kordijazi, A., Rohatgi, P. K., Rohatgi, P. K., Nosonovsky, M., & Nosonovsky, M. (2022a). Application of Triboinformatics Approach in Tribological Studies of Aluminum Alloys and Aluminum-Graphite Metal Matrix Composites. *The Minerals, Metals & Materials Series*.

Hasan, S., Hasan, S., Kordijazi, A., Kordijazi, A., Rohatgi, P. K., Rohatgi, P. K., Nosonovsky, M., & Nosonovsky, M. (2022b). Triboinformatics Approach for Friction and Wear Prediction of Al-Graphite Composites Using Machine Learning Methods. *Journal of Tribology-Transactions of The Asme*.

Himanen, L., Jäger, M. O. J., Morooka, E. v, Federici Canova, F., Ranawat, Y. S., Gao, D. Z., Rinke, P., & Foster, A. S. (2020). DScribe: Library of descriptors for machine learning in materials science. *Computer Physics Communications*, *247*, 106949.

Holmberg, K., & Erdemir, A. (2017). Influence of tribology on global energy consumption, costs and emissions. Friction, 5(3), 263–284.

Hutchings, I., & Shipway, P. (2017). Tribology: friction and wear of engineering materials. Butterworth-heinemann.

Ibrahim, M. S., Sulaiman, M. H., Samin, R., Yaakob, Y., Kamis, S. L., Ridzuan, M. J. M., Pauzi, A. A., Sukindar, N. A., & Bienk, K. (2024). Tool wear of DLC coating as toplayered to CrN, TiAlSiN, TiAlN coatings in machining of steel and aluminum alloys. *Wear*, *558–559*, 205574.

Ideris, M. H., Kamaruddin, S., Sulaiman, M. H., & Sukindar, N. A. (2023). Effects of Coating and Lubrication on Friction and Wear for Metal-to Metal Application. 1(1), 52–62.

Inspektor, A., & Salvador, P.A. (2014). Architecture of PVD coatings for metalcutting applications: A review. Surface & Coatings Technology, 257, 138-153.

Jia, B., Wan, Q., Yan, L., Luo, Y., Wei, Q., Niu, C., Yang, B., Li, S., & Meng, L. (2024). Tribological properties and machine learning prediction of FeCoCrNiAlN high entropy coatings. *Surface and Coatings Technology*, *477*, 130341.

Kamel, B. m, Tirth, V., Algahtani, A., Shiba, M., Mobasher, A., Abu Hashish, H., & Dabees, S. (2021). Optimization of the Rheological Properties and Tribological Performance of SAE 5w-30 Base Oil with Added MWCNTs. Lubricants, 9.

Kennedy, F. E. (1984). Thermal and thermomechanical effects in dry sliding. Wear, 100(1–3), 453–476

La, D. D., Truong, T., Pham, T., Vo, H. T., Tran, N., Nguyen, T., Nadda, A., Tung, N. T., Chang, S.-W., Chung, W., & Nguyen, D. D. (2020). Scalable Fabrication of Modified Graphene Nanoplatelets as an Effective Additive for Engine Lubricant Oil. *Nanomaterials*, *10*, 877.

Lansdown, A. R. (2004). Lubrication and lubricant selection: a practical guide. United Kingdom: ASME Press.

Lee, P., & Zhmud, B. (2021). Low Friction Powertrains: Current Advances in Lubricants and Coatings. *Lubricants*, *9*(8).

Łępicka, M., Grądzka-Dahlke, M., Pieniak, D., Pasierbiewicz, K., Kryńska, K., & Niewczas, A. (2020). Tribological performance of titanium nitride coatings: A comparative study on TiN-coated stainless steel and titanium alloy. *Wear*, *422–423*, 68–80.

Liñeira del Río, J. M., Guimarey, M. J. G., Prado, J. I., Lugo, L., López, E. R., & Comuñas, M. J. P. (2022). Improving the tribological performance of a biodegradable lubricant adding graphene nanoplatelets as additives. *Journal of Molecular Liquids*, *345*, 117797.

Liu, J., & Dumitrescu, C. E. (2019). Combustion partitioning inside a natural gas spark ignition engine with a bowl-in-piston geometry. *Energy Conversion and Management*, *183*, 73–83.

Ludema, K. C., & Ajayi, L. (2018). Friction, wear, lubrication: a textbook in tribology. CRC press.

Marian, M., Marian, M., Tremmel, S., & Tremmel, S. (2021). Current Trends and Applications of Machine Learning in Tribology—A Review. *Lubricants*.

Marlinda, A. R., Thien, G. S. H., Shahid, M., Ling, T. Y., Hashem, A., Chan, K.-Y., & Johan, M. R. (2023). Graphene as a Lubricant Additive for Reducing Friction and Wear in Its Liquid-Based Form. *Lubricants*, *11*(1).

Matt, H. (2016, October 28). What is HIPIMS? High Power Impulse Magnetron Sputtering. Semicore.com. Retrieved March 31, 2024, from https://www.semicore.com/.

Mattox, D. M. (2010). Handbook of Physical Vapor Deposition (PVD) Processing (Second Edition), William Andrew Publishing,

Oganesova, E. Yu., Lyadov, A. S., & Parenago, O. P. (2018). Nanosized Additives to Lubricating Materials. *Russian Journal of Applied Chemistry*, *91*(10), 1559–1573.

Ogunsanya, M., Isichei, J., & Desai, S. (2023). Grid search hyperparameter tuning in additive manufacturing processes. *Manufacturing Letters*, *35*, 1031–1042.

Özkan, D., Erarslan, Y., Sulukan, E., Kara, L., Alper Yılmaz, M., & Yağcı, M. B. (2018). Tribological Behavior of TiAlN, AlTiN, and AlCrN Coatings at Boundary Lubricating Condition. *Tribology Letters*, *66*(4), 152.

Pasha, M. B., Rao, R. N., Ismail, S., Gupta, M., & Prasad, P. S. (2024). Tribo-informatics approach to predict wear and friction coefficient of Mg/Si3N4 composites using machine learning techniques. *Tribology International*, *196*, 109696.

Rajput, A. S., & Das, S. (2023). A machine learning approach to predict the wear behaviour of steels. *Tribology International*, *185*, 108500.

Richard, C. (2013). Tribological Coatings for High-Temperature Applications." In Encyclopedia of Tribology, edited by Q.J. Wang and Y.-W. Chung, 3778–3787. Boston, MA: Springer US.

Rosenkranz, A., Marian, M., Profito, F., Aragon, N., & Shah, R. (2021). The Use of Artificial Intelligence in Tribology – A Perspective. *Lubricants*, *9*.

Rui, L. M., Sulaiman, M. H., Ashman, M., & Azizan, H. (2023). *Enhancing physical , mechanical , tribological and contact characteristics of water-based lubrication using ceramic nanomaterials MgO and SiC for metal-to-metal sliding interfaces*. *39*(October), 51–68.

Sharuddin MH, Sulaiman MH., Kamaruddin S, et al. Properties and tribological evaluation of graphene and fullerene nanoparticles as additives in oil lubrication. Proceedings of the Institution of Mechanical Engineers, Part J: Journal of Engineering Tribology. 2023;237(8):1647-1656.

Shen, G., Fang, F., & Kang, C. (2018). Tribological Performance of Bioimplants: A Comprehensive Review. *Nanotechnology and Precision Engineering*, *1*(2), 107–122.

Singh, S. K., Chattopadhyaya, S., Pramanik, A., Kumar, S., & Basak, A. K. (2019). Effect of lubrication on the wear behaviour of CrN coating deposited by PVD process. *International Journal of Surface Science and Engineering*, *13*(1), 60–78.

Srinath, M. K., & Prasad, M. S. G. (2020). Wear and corrosion resistance of titanium carbo-nitride coated Al-7075 produced through PVD. *Bulletin of Materials Science*, *43*(1), 108.

Stachowiak, G., W. (2005). Wear - Materials, Mechanisms and Practice. (1st ed.) England: Wiley.

Sudeep, U., Tandon, N., and Pandey, R. K. (2015). Performance of Lubricated Rolling/Sliding Concentrated Contacts With Surface Textures: A Review. ASME. J. Tribol. 137(3), 031501

Tong, Zhe & Ma, Qiang & Ni, Yuquan & Mei, Tangjie & Li, Jianhui & Dong, Guangneng. (2019). Tribological properties of carbon fabric reinforced phenolic-based composites containing CNTs@MoS2 hybrids. Journal of Materials Science. 54.

Xie, Z., & Zhu, W. (2021). Theoretical and experimental exploration on the micro asperity contact load ratios and lubrication regimes transition for water-lubricated stern tube bearing. *Tribology International*, *164*, 107105.

Waqas, M., Zahid, R., Bhutta, M. U., Khan, Z. A., & Saeed, A. (2021). A Review of Friction Performance of Lubricants with Nano Additives. *Materials (Basel, Switzerland)*, *14*(21).

Yadav, R., Meena, A., Lee, H.-H., Lee, S.-Y., & Park, S.-J. (2023). Tribological behavior of dental resin composites: A comprehensive review. *Tribology International*, *190*, 109017.

Yi, J., Xiong, J., Guo, Z., Yang, T., Liu, J., You, Q., Fang, D., Yu, Z., Gou, S., & Chen, S. (2022). Growth, mechanical properties, and tribological performance of TiAlN/NbN and NbN/TiAlN bilayer coatings. *Ceramics International*, *48*(5), 6208–6217.

Zhang, J., Li, Z., Wang, Y., Zhou, S., Wang, Y., Zeng, Z., & Li, J. (2020). A new method to improve the tribological performance of metal nitride coating: A case study for CrN coating. *Vacuum*, *173*, 109158.

Zhang, Y., Ma, Z., Feng, Y., Diao, Z., & Liu, Z. (2021). The Effects of Ultra-Low Viscosity Engine Oil on Mechanical Efficiency and Fuel Economy. *Energies*, *14*, 2320.

APPENDIX I : DATA SHEET (UNCOATED STEEL BLOCK)

Bearing Steel (Block) - Bearing Steel (Ring)									
Steel - Steel (SAE 0W20)				TNB rate	21.80 sen/kWh				
Temp : Room Temperature									
Duration : 20 minutes									
Time (sec)	**0**	**60**	**120**	**180**	**240**	**300**	**360**	**600**	**900**
Load (kg) (CONSTANT)	0	**1.8**	**1.8**	**1.8**	**1.8**	**1.8**	**1.8**	**1.8**	**1.8**
Power (W)	0	233.7	261.4	267.1	261.9	260.4	258.9	277.9	282.1
RPM		480	487	486.8	486.4	486.5	487.6	485.2	485.1
Count	0	487	1023	1463	1963	2440	2997	4870	7319
Block Mass (g) BEFORE TEST	0.0000	16.5061	16.4750	16.4459	16.4286	16.5110	16.4945	16.4693	16.4189
Block Mass (g) AFTER TEST	0.0000	16.4750	16.4459	16.4286	16.4110	16.4945	16.4693	16.4189	16.3955
Temp measurement	30								
Temp measurement (thermal camera)	30	66.7	77.1	80.9	84.8	101.2	103.4	122.1	129.5
Electric cost (sen)	0	0.0	0.0	0.0	0.0	0.0	0.0	0.0	0.0
FRICTION									
Angular speed $\omega=2\pi N/60$ (rad/s)	0	50.3	51.0	51.0	50.9	51.0	51.1	50.8	50.8
Torque $T=P/\omega$ (Nm)	0	4.6	5.1	5.2	5.1	5.1	5.1	5.5	5.6
Weight $W = mg = F_N$ (N)	0	17.7	17.7	17.7	17.7	17.7	17.7	17.7	17.7
Friction Force $F_f=T/R$ (N)	0	232.4	256.2	261.9	257.1	255.5	253.5	273.4	277.6
Friction Coef $\mu=F_f/F_N$	0	0.076	0.069	0.067	0.069	0.069	0.070	0.065	0.064
WEAR (Archard model, 1957)									
Distance $L=2\pi R$ x rev (m)	0	61	129	184	247	307	377	612	920
Volume Loss $W=m/\rho$ (mm3)	0	3.982074	3.7259923	2.2151088	2.2535211	2.11267606	3.22663252	6.45326504	2.996159
Wear rate $K=WH/F_NL$ (mm3/Nm)	0.000	3.210	1.430	0.594	0.451	0.340	0.423	0.520	0.161
MICROSCOPE									

Wear measure a (mm)		8.7	8.743	7.613	7.538	8.444	8.359	7.517	7.602
Wear measure b (mm)		4.936	4.808	4.339	4.179	4.691	4.542	4.169	4.211
Worn area a x b (mm^2)	0	42.9432	42.036344	33.032807	31.501302	39.610804	37.966578	31.338373	32.01202
Brugger value (N/mm^2)	0	0.411194	0.4200651	0.5345595	0.5605483	0.44578747	0.46509327	0.56346256	0.551605
Steel - Steel (SAE 5W30)				TNB rate	21.80 sen/kWh				
Temp : Room Temperature									
Duration : 20 minutes									
Time (sec)	**0**	**60**	**120**	**180**	**240**	**300**	**600**	**900**	
Load (kg) (CONSTANT)	0	**1.8**	**1.8**	**1.8**	**1.8**	**1.8**	**1.8**	**1.8**	
Power (W)	0	253.3	256.2	255.7	261.2	262	273	272.4	
RPM		488.4	484.3	488.2	478.7	486.3	487.1	487.3	
Count	0	499	990	1345	1971	2497	4390	7276	
Block Mass (g) BEFORE TEST	0	16.4693	16.5743	16.5479	16.5226	16.5091	16.4998	16.4811	
Block Mass (g) AFTER TEST	0	16.4442	16.5479	16.5226	16.5091	16.4998	16.4811	16.461	
Temp measurement (wire)	30								
Temp measurement (thermal camera)	30	73.4	79.6	86	94.2	97.2	111.1	120.4	
Electric cost (sen)	0	0.0	0.0	0.0	0.0	0.0	0.0	0.0	
FRICTION									
Angular speed $\omega=2\pi N/60$ (rad/s)	0	51.2	50.7	51.1	50.1	50.9	51.0	51.0	
Torque $T=P/\omega$ (Nm)	0	5.0	5.1	5.0	5.2	5.1	5.4	5.3	
Weight W = mg = F_N (N)	0	17.7	17.7	17.7	17.7	17.7	17.7	17.7	
Friction Force $F_f=T/R$ (N)	0	247.6	252.6	250.0	260.5	257.2	267.6	266.9	
Friction Coef $\mu=F_f/F_N$	0	0.071	0.070	0.071	0.068	0.069	0.066	0.066	
WEAR (Archard model, 1957)									
Distance $L=2\pi R$ x rev (m)	0	63	124	169	248	314	552	914	
Volume Loss $W=m/\rho$ (mm3)	0	3.213828	3.3802817	3.2394366	1.7285531	1.19078105	2.3943662	2.57362356	
Wear rate $K=WH/F_NL$ (mm3/Nm)	0.000	2.528	1.340	0.946	0.344	0.187	0.214	0.139	
MICROSCOPE									

Wear measure a (mm)		8.114	8.359	8.316	7.218	6.418	7.101	7.346	
Wear measure b (mm)		4.606	4.627	4.531	3.945	3.518	3.945	3.977	
Worn area a x b (mm^2)	0	37.37308	38.677093	37.679796	28.47501	22.578524	28.013445	29.215042	
Brugger value (N/mm^2)	0	0.472479	0.4565493	0.4686331	0.6201227	0.78207061	0.63034018	0.60441467	
Steel - Steel (GRAPHENE OIL)				TNB rate	21.80 sen/kWh				
Temp : Room Temperature									
Duration : 20 minutes									
Time (sec)	**0**	**60**	**120**	**180**	**240**	**300**	**600**	**900**	
Load (kg) **(CONSTANT)**	0	**1.8**	**1.8**	**1.8**	**1.8**	**1.8**	**1.8**	**1.8**	
Power (W)	0	268.4	266.5	269.5	274.7	276.4	263.3	271.9	
RPM		487.4	487.8	487.5	487.6	487.6	488.4	488.7	
Count	0	506	988	1475	1960	2448	4907	7200	
Block Mass (g) BEFORE TEST	0	16.5229	16.5228	16.5227	16.5226	16.5224	16.5223	16.522	
Block Mass (g) AFTER TEST	0	16.5228	16.5227	16.5226	16.5224	16.5223	16.522	16.5215	
Temp measurement (wire)	30								
Temp measurement (thermal camera)	30	62.9	64.2	73.9	81.4	89.8	94.7	93.5	
Electric cost (sen)	0	0.0	0.0	0.0	0.0	0.0	0.0	0.0	
FRICTION									
Angular speed $\omega=2\pi N/60$ (rad/s)	0	51.0	51.1	51.1	51.1	51.1	51.2	51.2	
Torque $T=P/\omega$ (Nm)	0	5.3	5.2	5.3	5.4	5.4	5.1	5.3	
Weight $W = mg = F_N$ (N)	0	17.7	17.7	17.7	17.7	17.7	17.7	17.7	
Friction Force $F_f=T/R$ (N)	0	262.9	260.8	263.9	269.0	270.6	257.4	265.6	
Friction Coef $\mu=F_f/F_N$	0	0.067	0.068	0.067	0.066	0.065	0.069	0.066	
WEAR (Archard model, 1957)									
Distance $L=2\pi R$ x rev (m)	0	64	124	185	246	308	617	905	
Volume Loss $W=m/\rho$ (mm3)	0	0.012804	0.0128041	0.0128041	0.0256082	0.0128041	0.03841229	0.06402049	
Wear rate $K=WH/F_NL$ (mm3/Nm)	0.00	0.010	0.005	0.003	0.005	0.002	0.003	0.003	
	0.00	9.934	5.088	3.408	5.129	2.053	3.073	3.491	

MICROSCOPE									
Wear measure a (mm)		1.738	1.608	1.695	2.015	1.887	2.154	2.559	
Wear measure b (mm)		1.109	1.119	1.077	1.258	1.194	1.333	1.535	
Worn area a x b (mm^2)	0	1.927442	1.799352	1.825515	2.53487	2.253078	2.871282	3.928065	
	0	19.2744	17.99352	18.25515	25.3487	22.53078	28.71282	39.28065	
Brugger value (N/mm^2)	0	9.161365	9.8135329	9.6728868	6.9660377	7.8372786	6.14986616	4.49534313	
Steel - Steel (FULLERENE)				TNB rate	21.80 sen/kWh				
Temp : Room Temperature									
Duration : 20 minutes									
Time (sec)	**0**	**60**	**120**	**180**	**240**	**300**	**600**	**900**	
Load (kg) (CONSTANT)	0	**1.8**	**1.8**	**1.8**	**1.8**	**1.8**	**1.8**	**1.8**	
Power (W)	0	241.4	248	251.9	256.2				
RPM		490	490	488	490				
Count	0	482	995	1480	1959				
Block Mass (g) BEFORE TEST	0	16.5758	16.5475	16.5067	16.4855				
Block Mass (g) AFTER TEST	0	16.5475	16.5067	16.4855	16.4483				
Temp measurement (wire)	30								
Temp measurement (thermal camera)	30	68	82	80	101				
Electric cost (sen)	0	0.0	0.0	0.0	0.0	0.0	0.0	0.0	
FRICTION									
Angular speed $\omega=2\pi N/60$ (rad/s)	0	51.3	51.3	51.1	51.3	0.0	0.0	0.0	
Torque $T=P/\omega$ (Nm)	0	4.7	4.8	4.9	5.0				
Weight $W = mg = F_N$ (N)	0	17.7	17.7	17.7	17.7	17.7	17.7	17.7	
Friction Force $F_f=T/R$ (N)	0	235.2	241.6	246.4	249.6				
Friction Coef $\mu=F_f/F_N$	0	0.075	0.073	0.072	0.071				
WEAR (Archard model, 1957)									
Distance $L=2\pi R$ x rev (m)	0	61	125	186	246	500	800	900	

Volume Loss W=m/ρ (mm3)	0	3.62356	5.2240717	2.7144686	4.7631242	0	0	0	
Wear rate K=WH/F_NL (mm3/Nm)	0.000	2.951	2.061	0.720	0.955	0.000	0.000	0.000	
MICROSCOPE									
Wear measure a (mm)		5.331	8.615	7.485	8.881				
Wear measure b (mm)		3.028	4.872	4.062	4.915				
Worn area a x b (mm^2)	0	16.14227	41.97228	30.40407	43.650115	0	0	0	
Brugger value (N/mm^2)	0	1.093898	0.4207062	0.5807775	0.404535				

APPENDIX II : DATA SHEET (COATED STEEL BLOCK)

CrN (graphene oil)				TNB rate	21.80 sen/kWh					
Temp : Room Temperature										
Duration : 20 minutes										
Time (sec)	**0**	**60**	**120**	**180**	**240**	**300**	**600**	**900**	**1800**	**3600**
Load (kg) (CONSTANT)	0	**1.8**	**1.8**	**1.8**	**1.8**	**1.8**	**1.8**	**1.8**	**1.8**	**1.8**
Power (W)	0	254.1	262.1	263.8	266.8	265.6	264.2	265.2	259.4	277.6
RPM		487	487	487	487	487	486	485	485	485
Count	0	493	968	1457	1950	2468	4893	6315	14517	29130
Block Mass (g) BEFORE TEST	0	9.9347	9.9345	9.9306	9.9284	9.924	9.9238	9.923	9.9003	9.8795
Block Mass (g) AFTER TEST	0	9.9345	9.9306	9.9284	9.924	9.9238	9.923	9.9003	9.8795	9.3254
Temp measurement(wire)	30	42.4	58.8	54.9	66.3	69.6	80.6	107	114.9	157.2
Temp measurement (thermal camera)	30	58.3	60.2	71.5	83	91	107.3	117.8	117.8	117.8
Electric cost (sen)	0	0.0	0.0	0.0	0.0	0.0	0.0	0.0	0.0	0.0
FRICTION										
Angular speed $\omega=2\pi N/60$ (rad/s)	0	51.0	51.0	51.0	51.0	51.0	50.9	50.8	50.8	50.8
Torque $T=P/\omega$ (Nm)	0	5.0	5.1	5.2	5.2	5.2	5.2	5.2	5.1	5.5
Weight $W = mg = F_N$ (N)	0	17.7	17.7	17.7	17.7	17.7	17.7	17.7	17.7	17.7
Friction Force $F_f=T/R$ (N)	0	249.1	256.9	258.6	261.5	260.4	259.5	261.0	255.3	273.3
Friction Coef $\mu=F_f/F_N$	0	0.071	0.069	0.068	0.068	0.068	0.068	0.068	0.069	0.065
WEAR (Archard model, 1957)										
Distance $L=2\pi R$ x rev (m)	0	62	122	183	245	310	615	794	1824	3661
Volume Loss $W=m/\rho$ (mm3)	0	0.02561	0.49936	0.28169	0.56338	0.02561	0.10243	2.90653	2.66325	70.9475
Wear rate $K=WH/F_NL$ (mm3/Nm)	0.000	0.020	0.203	0.076	0.113	0.004	0.008	0.181	0.072	0.956
MICROSCOPE										
Wear measure a (mm)		4.19	6.504	4.968	6.44	4.531	4.51	5.565	9.169	16.281
Wear measure b (mm)		1.813	2.836	2.122	2.889	2.058	2.079	2.729	4.062	6.765
Worn area a x b (mm^2)	0	7.59647	18.4453	10.5421	18.6052	9.3248	9.37629	15.1869	37.2445	110.141
Brugger value (N/mm^2)	0	2.3245	0.95731	1.675	0.94909	1.89366	1.88326	1.16271	0.47411	0.16032
TiAlSN (graphene oil)				TNB rate	21.80 sen/kWh					

Temp : Room Temperature										
Duration : 20 minutes										
Time (sec)	**0**	**60**	**120**	**180**	**240**	**300**	**600**	**900**	**1800**	**3600**
Load (kg) (CONSTANT)	0	**1.8**	**1.8**	**1.8**	**1.8**	**1.8**	**1.8**	**1.8**	**1.8**	**1.8**
Power (W)	0	242.1	241.7	251.5	250.2	254.4	260.6	256.3	264.9	265.9
RPM		489	488	488	488	488	485	485	487	487
Count	0	505	984	1470	1963	2452	4867	7259	14629	29128
Block Mass (g) BEFORE TEST	0	10.4867	10.4865	10.4866	10.4865	10.4864	10.4863	10.4859	10.4856	10.4852
Block Mass (g) AFTER TEST	0	10.4866	10.4865	10.4865	10.4864	10.4863	10.4859	10.4856	10.4852	10.4837
Temp measurement (wire)	30	43.4	52.9	62.3	63.9	64.6	100.4	102	102	135.5
Temp measurement (thermal camera)	30	48.8	56.9	71.6	75.6	83.9	100.6	119.6	121.7	155.8
Electric cost (sen)	0	0.0	0.0	0.0	0.0	0.0	0.0	0.0	0.0	0.0
FRICTION										
Angular speed $\omega=2\pi N/60$ (rad/s)	0	51.2	51.1	51.1	51.1	51.1	50.8	50.8	51.0	51.0
Torque $T=P/\omega$ (Nm)	0	4.7	4.7	4.9	4.9	5.0	5.1	5.0	5.2	5.2
Weight $W = mg = F_N$ (N)	0	17.7	17.7	17.7	17.7	17.7	17.7	17.7	17.7	17.7
Friction Force $F_f=T/R$ (N)	0	236.4	236.5	246.0	244.8	248.9	256.5	252.3	259.7	260.7
Friction Coef $\mu=F_f/F_N$	0	0.075	0.075	0.072	0.072	0.071	0.069	0.070	0.068	0.068
WEAR (Archard model, 1957)										
Distance $L=2\pi R$ x rev (m)	0	63	124	185	247	308	612	912	1839	3661
Volume Loss $W=m/\rho$ (mm3)	0	0.0128	0	0.0128	0.0128	0.0128	0.05122	0.03841	0.05122	0.19206
Wear rate $K=WH/F_NL$ (mm3/Nm)	0.000	0.010	0.000	0.003	0.003	0.002	0.004	0.002	0.001	0.003
MICROSCOPE										
Wear measure a (mm)		2.26	1.599	2.058	2.047	2.868	2.932	3.071	3.358	6.461
Wear measure b (mm)		1.034	0.746	0.896	0.896	1.258	1.386	1.557	1.621	2.889
Worn area a x b (mm^2)	0	2.33684	1.19285	1.84397	1.83411	3.60794	4.06375	4.78155	5.44332	18.6658
Brugger value (N/mm^2)	0	7.55636	14.8032	9.57609	9.62755	4.8942	4.34525	3.69295	3.24398	0.94601
TiN (graphene oil)				TNB rate	21.80 sen/kWh					
Temp : Room Temperature										
Duration : 20 minutes										
Time (sec)	**0**	**60**	**120**	**180**	**240**	**300**	**600**	**900**	**1800**	**3600**
Load (kg) (CONSTANT)	0	**1.8**	**1.8**	**1.8**	**1.8**	**1.8**	**1.8**	**1.8**	**1.8**	**1.8**
Power (W)	0	248.1	248.5	251.6	256.6	258.8	265.3	266.8	259.5	263.7

RPM		488	487	487	487	487	487	487	487	487
Count	0	502	1013	1490	1987	2448	4873	7276	14579	29155
Block Mass (g) BEFORE TEST	0	10.3705	10.3704	10.3703	10.3702	10.3701	10.3699	10.3696	10.3689	10.3672
Block Mass (g) AFTER TEST	0	10.3704	10.3703	10.3702	10.3701	10.3699	10.3696	10.3689	10.3672	10.3555
Temp measurement (wire)	30	48.2	51.6	72.7	75.4	90.6	108.4	126.2	146.4	132
Temp measurement (thermal camera)	30	49.5	62.7	79.5	96.5	108.7	131.4	136.6	146	154.8
Electric cost (sen)	0	0.0	0.0	0.0	0.0	0.0	0.0	0.0	0.0	0.0
FRICTION									
Angular speed $\omega=2\pi N/60$ (rad/s)	0	51.1	51.0	51.0	51.0	51.0	51.0	51.0	51.0	51.0
Torque $T=P/\omega$ (Nm)	0	4.9	4.9	4.9	5.0	5.1	5.2	5.2	5.1	5.2
Weight $W = mg = F_N$ (N)	0	17.7	17.7	17.7	17.7	17.7	17.7	17.7	17.7	17.7
Friction Force $F_f=T/R$ (N)	0	242.7	243.6	246.6	251.5	253.7	260.1	261.5	254.4	258.5
Friction Coef $\mu=F_f/F_N$	0	0.073	0.072	0.072	0.070	0.070	0.068	0.068	0.069	0.068
WEAR (Archard model, 1957)									
Distance $L=2\pi R$ x rev (m)	0	63	127	187	250	308	612	914	1832	3664
Volume Loss $W=m/\rho$ (mm3)	0	0.0128	0.0128	0.0128	0.0128	0.02561	0.03841	0.08963	0.21767	1.49808
Wear rate $K=WH/F_NL$ (mm3/Nm)	0.000	0.010	0.005	0.003	0.003	0.004	0.003	0.005	0.006	0.020
MICROSCOPE									
Wear measure a (mm)		2.644	2.484	2.655	2.751	2.348	4.073	4.808	5.16	8.615
Wear measure b (mm)		1.056	1.13	1.162	1.247	1.461	1.749	2.058	2.324	3.785
Worn area a x b (mm^2)	0	2.79206	2.80692	3.08511	3.4305	3.43043	7.12368	9.89486	11.9918	32.6078
Brugger value (N/mm^2)	0	6.32435	6.29088	5.72362	5.14736	5.14746	2.47878	1.78456	1.4725	0.54153
DLC (graphene oil)				TNB rate	21.80	sen/kWh				
Temp : Room Temperature									
Duration : 20 minutes									
Time (sec)	**0**	**60**	**120**	**180**	**240**	**300**	**600**	**900**	**1800**	**3600**
Load (kg) (CONSTANT)	0	**1.8**	**1.8**	**1.8**	**1.8**	**1.8**	**1.8**	**1.8**	**1.8**	**1.8**
Power (W)	0	247.6	254.8	263.3	265.5	272.6	271.8	272.1	267.8	271.9
RPM		490	490	490	487	487	487	486	486	484
Count	0	493	973	1464	1960	2470	4866	7290	14567	29239
Block Mass (g) BEFORE TEST	0	10.1115	10.1114	10.1113	10.1112	10.1111	10.1109	10.1108	10.1107	10.1104
Block Mass (g) AFTER TEST	0	10.1114	10.1113	10.1112	10.1111	10.1109	10.1108	10.1107	10.1104	10.1055
Temp measurement (wire)	30	48.2	51.6	72.7	75.4	90.6	108.4	126.2	146.4	132

Temp measurement (thermal camera)	30	49.5	62.7	79.5	96.5	108.7	131.4	136.6	146	154.8
Electric cost (sen)	0	0.0	0.0	0.0	0.0	0.0	0.0	0.0	0.0	0.0
FRICTION										
Angular speed ω=2πN/60 (rad/s)	0	51.3	51.3	51.3	51.0	51.0	51.0	50.9	50.9	50.7
Torque T=P/ω (Nm)	0	4.8	5.0	5.1	5.2	5.3	5.3	5.3	5.3	5.4
Weight W = mg = F_N (N)	0	17.7	17.7	17.7	17.7	17.7	17.7	17.7	17.7	17.7
Friction Force F_f=T/R (N)	0	241.2	248.2	256.5	260.3	267.2	266.4	267.3	263.1	268.2
Friction Coef $\mu=F_f/F_N$	0	0.073	0.071	0.069	0.068	0.066	0.066	0.066	0.067	0.066
WEAR (Archard model, 1957)										
Distance L=2πR x rev (m)	0	62	122	184	246	310	612	916	1831	3675
Volume Loss W=m/ρ (mm3)	0	0.0128	0.0128	0.0128	0.0128	0.02561	0.0128	0.0128	0.03841	0.6274
Wear rate K=WH/F_NL (mm3/Nm)	0.000	0.010	0.005	0.003	0.003	0.004	0.001	0.001	0.001	0.008
MICROSCOPE										
Wear measure a (mm)		2.42	2.527	2.26	1.695	2.079	2.57	3.988	3.657	7.165
Wear measure b (mm)		1.077	1.066	1.098	0.864	1.056	1.173	1.791	1.791	3.199
Worn area a x b (mm^2)	0	2.60634	2.69378	2.48148	1.46448	2.19542	3.01461	7.14251	6.54969	22.9208
Brugger value (N/mm^2)	0	6.77502	6.5551	7.11591	12.0575	8.04309	5.85747	2.47224	2.69601	0.77039
AlTiN (graphene oil)				TNB rate	21.80 sen/kWh					
Temp : Room Temperature										
Duration : 20 minutes										
Time (sec)	**0**	**60**	**120**	**180**	**240**	**300**	**600**	**900**	**1800**	**3600**
Load (kg) (CONSTANT)	0	**1.8**	**1.8**	**1.8**	**1.8**	**1.8**	**1.8**	**1.8**	**1.8**	**1.8**
Power (W)	0	243.3	251.1	262.8	257	269.2	267.5	260.2	261	260
RPM		490	490	490	490	490	489	489	485	486
Count	0	495	987	1485	1959	2450	4858	7312	14608	29152
Block Mass (g) BEFORE TEST	0	10.1785	10.1784	10.1783	10.1781	10.1782	10.178	10.1779	10.1778	10.1767
Block Mass (g) AFTER TEST	0	10.1784	10.1883	10.1782	10.178	10.1781	10.1779	10.1778	10.1775	10.1757
Temp measurement(wire)	30	40	49.5	55.9	59.3	65.2	77.7	95.9	96.8	101.7
Temp measurement (thermal camera)	30	41	56.7	65.9	71.2	84.3	116.9	121.5	126.4	123.7
Electric cost (sen)	0	0.0	0.0	0.0	0.0	0.0	0.0	0.0	0.0	0.0
FRICTION										
Angular speed ω=2πN/60 (rad/s)	0	51.3	51.3	51.3	51.3	51.3	51.2	51.2	50.8	50.9

Torque T=P/ω (Nm)	0	4.7	4.9	5.1	5.0	5.2	5.2	5.1	5.1	5.1
Weight W = mg = F_N (N)	0	17.7	17.7	17.7	17.7	17.7	17.7	17.7	17.7	17.7
Friction Force F_f=T/R (N)	0	237.0	244.6	256.0	250.4	262.3	261.2	254.0	256.9	255.4
Friction Coef $\mu=F_f/F_N$	0	0.074	0.072	0.069	0.071	0.067	0.068	0.070	0.069	0.069
WEAR (Archard model, 1957)										
Distance L=2πR x rev (m)	0	62	124	187	246	308	611	919	1836	3664
Volume Loss W=m/ρ (mm3)	0	0.0128	-1.2676	0.0128	0.0128	0.0128	0.0128	0.0128	0.03841	0.12804
Wear rate K=WH/F_NL (mm3/Nm)	0.000	0.010	-0.504	0.003	0.003	0.002	0.001	0.001	0.001	0.002
MICROSCOPE										
Wear measure a (mm)		1.855	1.905	1.717	1.94	2.303	2.303	2.431	3.092	3.198
Wear measure b (mm)		1.013	0.906	0.757	0.981	0.917	0.917	1.109	1.61	1.731
Worn area a x b (mm^2)	0	1.87912	1.72593	1.29977	1.90314	2.11185	2.11185	2.69598	4.97812	5.53574
Brugger value (N/mm^2)	0	9.39698	10.231	13.5855	9.27835	8.36139	8.36139	6.54975	3.54712	3.18982
TICN - Steel (GRAPHENE)				TNB rate	21.80 sen/kWh					
Temp : Room Temperature										
Duration : 20 minutes										
Time (sec)	**0**	**60**	**120**	**180**	**240**	**300**	**600**	**900**	**1800**	**3600**
Load (kg) (CONSTANT)	0	**1.8**	**1.8**	**1.8**	**1.8**	**1.8**	**1.8**	**1.8**	**1.8**	**1.8**
Power (W)	0	264	266.8	267.1	268.7	268.8	268.1	262.3	264.4	275.6
Power Consumption (kWh)	0	176.73	176.75	176.75	176.75	176.75	176.81	176.89	177.02	176.71
RPM		487	487	487	487	487	487	487	487	487
Count	0	504	1005	1468	1957	2443	4874	7437	14612	29087
Block Mass (g) BEFORE TEST	0	10.4523	10.4521	10.4527	10.4526	10.4520	10.4518	10.4515	10.4512	10.4623
Block Mass (g) AFTER TEST	0	10.4521	10.4520	10.4526	10.4524	10.4518	10.4515	10.4512	10.4506	10.4523
Temp measurement (wire)	30	65.5	67.5	75.3	86	96.4	111	101	109.8	132.4
Temp measurement (thermal camera)	30	69.9	71.2	80.4	92.3	103.1	122.6	127.2	131.2	157.2
Electric cost (sen)	0	3852.7	3853.2	3853.2	3853.2	3853.2	3854.5	3856.2	3859.0	3852.3
FRICTION										
Angular speed ω=2πN/60 (rad/s)	0	51.0	51.0	51.0	51.0	51.0	51.0	51.0	51.0	51.0
Torque T=P/ω (Nm)	0	5.2	5.2	5.2	5.3	5.3	5.3	5.1	5.2	5.4
Weight W = mg = F_N (N)	0	17.7	17.7	17.7	17.7	17.7	17.7	17.7	17.7	17.7
Friction Force F_f=T/R (N)	0	258.8	261.5	261.8	263.4	263.5	262.8	257.1	259.2	270.2
Friction Coef $\mu=F_f/F_N$	0	0.068	0.068	0.067	0.067	0.067	0.067	0.069	0.068	0.065

WEAR (Archard model, 1957)										
Distance L=2πR x rev (m)	0	63	126	184	246	307	613	935	1836	3656
Volume Loss W=m/ρ (mm3)	0	0.026	0.013	0.013	0.026	0.026	0.038	0.038	0.077	1.280
Wear rate K=WH/F_NL (mm3/Nm)	0.000	0.020	0.005	0.003	0.005	0.004	0.003	0.002	0.002	0.017
MICROSCOPE										
Wear measure a (mm)		2.442	2.463	2.539	2.611	2.689	2.913	2.709	3.402	6.396
Wear measure b (mm)		1.034	1.077	1.085	1.093	1.100	1.181	1.263	1.629	2.790
Worn area a x b (mm^2)	0	2.52503	2.65265	2.75482	2.85382	2.9579	3.44025	3.42147	5.54186	17.8448
Brugger value (N/mm^2)	0	6.9932	6.6567	6.4099	6.1875	5.9698	5.1328	5.1609	3.1863	0.9895

PUBLICATIONS

Journal:

Sharuddin MH, Sulaiman MH., Kamaruddin S, et al. Properties and tribological evaluation of graphene and fullerene nanoparticles as additives in oil lubrication. Proceedings of the Institution of Mechanical Engineers, Part J: Journal of Engineering Tribology. 2023;237(8):1647-1656.

Poster Presentation:

M.H., Sharuddin, S. Kamaruddin, A.H. Dahnel, M.H. Sulaiman. Tribological performance of bearing steel under dry friction and lubricated sliding condition. 4th MYTRIBOS International Symposium organized by Malaysian Tribology Society (MYTRIBOS), August 2022.